

UWTHPH 2016-29
January 24, 2017

Perturbative corrections to $B \rightarrow D$ form factors in QCD

Yu-Ming Wang^{a,b}, Yan-Bing Wei^{c,d}, Yue-Long Shen^e, Cai-Dian Lü^{c,d}

^a School of Physics, Nankai University, 300071 Tianjin, China

^b Fakultät für Physik, Universität Wien, Boltzmanngasse 5, 1090 Vienna, Austria

^c Institute of High Energy Physics, CAS, P.O. Box 918(4) Beijing 100049, China

^d School of Physics, University of Chinese Academy of Sciences, Beijing 100049, China

^e College of Information Science and Engineering, Ocean University of China, Qingdao,
Shandong 266100, P.R. China

Abstract

We compute perturbative QCD corrections to $B \rightarrow D$ form factors at leading power in Λ/m_b , at large hadronic recoil, from the light-cone sum rules (LCSR) with B -meson distribution amplitudes in HQET. Applying the method of regions, QCD factorization for the vacuum-to- B -meson correlation function with an interpolating current for the D -meson is demonstrated explicitly at one loop with the power counting scheme $m_c \sim \mathcal{O}(\sqrt{\Lambda m_b})$. The hard functions entering the factorization formula are apparently identical to the matching coefficients of the QCD weak current $\bar{q} \gamma_\mu (1 - \gamma_5) b$ onto soft-collinear effective theory, due to the default counting rule for the charm-quark mass. The jet functions encoding information of the hard-collinear dynamics in the above-mentioned correlation function are complicated by the appearance of an additional hard-collinear scale m_c , compared to the counterparts entering the factorization formula of the vacuum-to- B -meson correction function for the construction of $B \rightarrow \pi$ form factors. Resummation of the parametrically large logarithms in the short-distance functions is achieved with the standard renormalization-group approach in the momentum space. Inspecting the resummation improved sum rules for the form factors of $B \rightarrow D\ell\nu$ indicates that perturbative corrections to the hard-collinear functions are more profound than that for the hard functions, with the default theory inputs, in the physical kinematic region. We further compute the subleading power correction induced by the three-particle quark-gluon distribution amplitudes of the B -meson at tree level employing the background gluon field approach. It turns out that the three-particle corrections to $B \rightarrow D$ form factors can only yield negligible impact numerically, approximately $\mathcal{O}(1\%)$. The LCSR predictions for the semileptonic $B \rightarrow D\ell\nu$ form factors are then extrapolated to the entire kinematic region with the z -series parametrization. Phenomenological implications of our determinations for the form factors $f_{BD}^{+,0}(q^2)$ are explored by investigating the (differential) branching fractions and the $R(D)$ ratio of $B \rightarrow D\ell\nu$ and by determining the CKM matrix element $|V_{cb}|$ from the total decay rate of $B \rightarrow D\mu\nu_\mu$.

1 Introduction

Precision calculations of the semileptonic heavy-to-heavy $B \rightarrow D\ell\nu$ decays are indispensable for a stringent test of the CKM matrix element $|V_{cb}|$ exclusively and for a deep understanding of the strong interaction mechanism in the heavy-quark system from both QCD and heavy-particle effective field theories. The long-standing tension between the exclusive and inclusive determinations of $|V_{cb}|$ [1] as well as the topical $R(D) \equiv \mathcal{BR}(B \rightarrow D\tau\nu_\tau)/\mathcal{BR}(B \rightarrow D\ell\nu)$ anomaly [2] necessitates further QCD calculations of $B \rightarrow D$ form factors with an increasing accuracy. Employing the heavy-quark expansion (HQE) technique, systematic studies of $B \rightarrow D$ form factors near zero recoil were performed including both perturbative QCD corrections and subleading power contributions (see [3] for a review). Very recently, the unquenched lattice-QCD calculations of $B \rightarrow D\ell\nu$ form factors near zero recoil were reported by the FNAL/MILC Collaboration [4] using the asqtad-improved fermions for the light valence quarks and the improved Wilson (“clover”) fermions for the heavy valence quarks and by the HPQCD Collaboration [5] independently applying the NRQCD action for bottom and the highly improved staggered quark action for charm quarks together with $N_f = 2 + 1$ MILC gauge configurations. However, extrapolating the HQE and lattice calculations of $B \rightarrow D$ form factors to the entire physical kinematic range can be only achieved with certain parametrizations for the momentum dependence of form factors, which introduce an additional source of theoretical uncertainties for the determination of $|V_{cb}|$. A direct QCD computation of the form factors of $B \rightarrow D\ell\nu$ at large recoil is therefore highly in demand to provide complementary information on the hadronic dynamics for a better understanding of the form-factor shapes. The major objective of this paper is to carry out perturbative QCD corrections to the two-particle contributions to $B \rightarrow D$ form factors at large recoil from the light-cone sum rules (LCSR) with B -meson distribution amplitudes (DA) following the techniques developed in [6–9], in an attempt to extend the leading-order calculation of the corresponding vacuum-to- B -meson correlation function performed in [10].

Applying the light-cone operator-product expansion (OPE) and parton-hadron duality, the LCSR approaches have been proven their usefulness in computing both the local and non-local hadronic matrix elements for the theory description of hadronic processes with large momentum transfer. Demonstrating QCD factorization for the vacuum-to- B -meson correlation function at leading power in Λ/m_b is evidently the first step in the construction of sum rules for $B \rightarrow D\ell\nu$ form factors. To this end, we need to establish the power counting scheme for the distinct momentum scales involved in the correlation function under consideration. In contrast to the correlation function for the heavy-to-light form factors, the appearance of an additional energy scale (the charm-quark mass) further complicates perturbative QCD factorization for the vacuum-to- B -meson correlation function with an interpolating current for the D -meson. Motivated by the mass hierarchy between the bottom and charm quarks numerically, we will adopt a novel power counting scheme $m_c \sim \mathcal{O}(\sqrt{\Lambda m_b})$, as implemented in the analysis of the inclusive semileptonic $B \rightarrow X_c\ell\nu$ decays [11, 12] with shape functions of the B -meson, instead of the popular counting scheme $m_c \sim \mathcal{O}(m_b)$ widely used in the heavy-quark physics (see, for instance [13, 14]). It is then apparent that the on-shell bottom-quark field, the charm-quark field appeared in the interpolating current for the D -meson and the external light-quark field can be identified as hard, hard-collinear and soft modes in QCD

following the convention of [15]. Despite the fact that implementing the light-cone OPE of the above-mentioned correlation function with three distinct momentum scales can be readily formulated in the framework of soft-collinear effective theory (SCET) including a massive hard-collinear quark [16, 17], we will employ an alternative strategy, namely the method of regions [18], to compute the short-distance functions entering the QCD factorization formulae for the considered correlation function, following closely [15, 19, 20].

With the specified power counting scheme for the charm-quark field, the hard functions from integrating out the dynamical fluctuations at the $\mathcal{O}(m_b)$ scale can be easily shown to be identical to the perturbative matching coefficients of the QCD weak current $\bar{q} \gamma_\mu (1 - \gamma_5) b$ in SCET, with the aid of the method of regions. However, the jet functions involved in the factorization formulae for the vacuum-to- B -meson correlation function develop a non-trivial dependence on the charm-quark mass, yielding an interesting source of the large-energy symmetry breaking effects for the vector and scalar $B \rightarrow D$ form factors. We will further verify explicitly at one loop that the jet functions for the vacuum-to- B -meson correlation function with an interpolating current for the D -meson, in the $m_c \rightarrow 0$ limit, can be reduced to the corresponding hard-collinear functions for the counterpart correlation function used in the construction of the sum rules for $B \rightarrow \pi$ form factors. QCD resummation for the parametrically large logarithms involved in the short-distance functions is achieved at next-to-leading-logarithmic (NLL) accuracy with the standard renormalization-group (RG) approach. In addition, we will evaluate the subleading power correction to the vacuum-to- B -meson correlation function from the three-particle B -meson DA at leading order in α_s , employing the light-cone OPE in the background field approach.

An alternative approach to compute the form factors of $B \rightarrow D\ell\nu$ from QCD sum rules was adopted in [21, 22] with the non-perturbative strong interaction dynamics encoded in the D -meson DA on the light cone. However, both calculations for the vacuum-to- D -meson correlation function with an interpolating current for the B -meson presented in [21, 22] were carried out at tree level without specifying the power counting scheme for the charm-quark field and without implementing the perturbative QCD constraints for the D -meson DA. Yet another QCD-based approach to evaluate $B \rightarrow D$ form factors in the framework of transverse-momentum-dependent (TMD) factorization was proposed in [23, 24] with the power counting $m_b \gg m_c \gg \Lambda$, which was further updated in [25] recently. Albeit with the technical progresses on the computations of perturbative matching coefficients [26–29], TMD factorization for hard exclusive processes is still not well established conceptually due to the lack of a definite power counting scheme for the intrinsic transverse momentum [30] and the Wilson-line structure of TMD wave functions needs to be constructed appropriately to avoid both the rapidity and pinch singularities in the infrared subtraction [31].

This paper is structured as follows. In Section 2 we will introduce the vacuum-to- B -meson correlation function for constructing the sum rules of $B \rightarrow D$ form factors and establish the power counting scheme for the external momenta in Λ/m_b . The essential ingredients to compute the semileptonic $B \rightarrow D\ell\nu$ form factors from the LCSR with B -meson DA, including QCD factorization for the considered correlation function and the hadronic dispersion relation, will be also presented by working out the tree-level sum rules at leading power in HQE. We will turn to demonstrate QCD factorization for the two-particle contributions to the vacuum-to- B -meson correlation function at $\mathcal{O}(\alpha_s)$ with the method of regions in Section 3, where the

hard coefficients and the jet functions appeared in the factorization formulae for the above-mentioned correlation function are computed manifestly at one loop. The NLL resummation improved sum rules for the two-particle contributions to $B \rightarrow D$ form factors will be also derived here and they constitute the main new results of this paper. In Section 4 we further calculate the three-particle contributions to the LCSR of $B \rightarrow D\ell\nu$ form factors at tree level, which will be shown to contribute only at subleading power in Λ/m_b with the power counting scheme adopted here. Phenomenological implications of the newly derived sum rules for the decay form factors of $B \rightarrow D\ell\nu$ will be explored in Section 5 with different models for B -meson DA, including determinations of the shape parameters for the vector and scalar $B \rightarrow D$ form factors with both the z -series expansion [32] and the Caprini-Lellouch-Neubert (CLN) parametrization [33], the differential branching fractions of $B \rightarrow D\ell\nu$ and $R(D)$ defined in the above, as well as the extraction of the CKM matrix element $|V_{cb}|$. We will conclude in Section 6 with a summary of main observations and a perspective on the future refinements. We collect some useful results of loop integrals for evaluating the vacuum-to- B -meson correlation function at one loop, present the spectral representations for the convolution integrals essential to construct the NLL LCSR of $B \rightarrow D$ form factors and display the lengthy coefficient functions entering the “effective” B -meson DA, absorbing the hard-collinear corrections at one loop, in Appendices A, B and C, respectively.

2 The framework

We briefly review the LCSR approach to compute $B \rightarrow D$ form factors with B -meson DA following the strategy presented in [15]. The vacuum-to- B -meson correlation function adopted to construct the sum rules for the form factors $f_{BD}^+(q^2)$ and $f_{BD}^0(q^2)$ is defined as

$$\Pi_\mu(n \cdot p, \bar{n} \cdot p) = i \int d^4x e^{ip \cdot x} \langle 0 | T \{ \bar{q}(x) \not{h} \gamma_5 c(x), \bar{c}(0) \gamma_\mu b(0) \} | \bar{B}(p_B) \rangle, \quad (1)$$

where $p_B \equiv m_B v$ indicates the four-momentum of the B -meson and p refers to the four-momentum carried by the interpolating current of the D -meson. We will work in the rest frame of the B -meson and introduce two light-cone vectors n_μ and \bar{n}_μ satisfying $n \cdot v = \bar{n} \cdot v = 1$ and $n \cdot \bar{n} = 2$. We will further employ the following power counting scheme

$$n \cdot p = \frac{m_B^2 + m_D^2 - q^2}{m_B} \sim \mathcal{O}(m_B), \quad |\bar{n} \cdot p| \sim \mathcal{O}(\Lambda), \quad m_c \sim \mathcal{O}\left(\sqrt{\Lambda m_b}\right), \quad (2)$$

at large hadronic recoil, where $q = p_B - p$ is the transfer momentum and Λ is a hadronic scale of order Λ_{QCD} . For the space-like interpolating momentum p , the leading power contribution to the correlation function (1) at tree level can be achieved by evaluating the diagram in figure 1 with the light-cone OPE and we obtain

$$\begin{aligned} \Pi_{\mu,2P}(n \cdot p, \bar{n} \cdot p) &= -i \tilde{f}_B(\mu) m_B \bar{n}_\mu \int_0^\infty d\omega \frac{\phi_B^-(\omega, \mu)}{\bar{n} \cdot p - \omega - \omega_c + i0} + \mathcal{O}(\alpha_s) \\ &= -i \tilde{f}_B(\mu) m_B \bar{n}_\mu \int_{\omega_c}^\infty d\omega' \frac{\phi_B^-(\omega' - \omega_c, \mu)}{\bar{n} \cdot p - \omega' + i0} + \mathcal{O}(\alpha_s), \end{aligned} \quad (3)$$

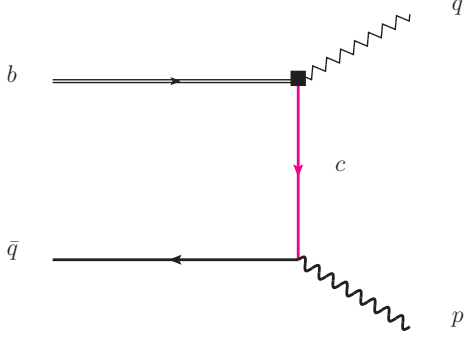


Figure 1: Diagrammatical representation of the two-particle contributions to the vacuum-to- B -meson correlation function $\Pi_\mu(n \cdot p, \bar{n} \cdot p)$ defined in (1) at tree level.

where $\omega_c = m_c^2/n \cdot p$ and the convolution integral in the second step corresponds to the spectral representation of the considered correlation function. It is apparent that (3) reproduces precisely the result for the corresponding correlation function defined with a pion interpolating current in the $m_c \rightarrow 0$ limit.

The light-cone DA of the B -meson in the coordinate space are defined as follows [34, 35]:

$$\begin{aligned} \langle 0 | (\bar{q} Y_s)_\beta (t \bar{n}) (Y_s^\dagger b_v)_\alpha (0) | \bar{B}(v) \rangle \\ = -\frac{i \tilde{f}_B(\mu) m_B}{4} \left\{ \frac{1+\not{v}}{2} \left[2 \tilde{\phi}_B^\pm(t, \mu) + (\tilde{\phi}_B^-(t, \mu) - \tilde{\phi}_B^+(t, \mu)) \not{n} \right] \gamma_5 \right\}_{\alpha\beta}, \end{aligned} \quad (4)$$

where b_v indicates the effective bottom-quark field in heavy-quark effective theory (HQET), the soft gauge link is given by

$$Y_s(t \bar{n}) = P \left\{ \text{Exp} \left[i g_s \int_{-\infty}^t dx \bar{n} \cdot A_s(x \bar{n}) \right] \right\}, \quad (5)$$

and $\phi_B^\pm(\omega, \mu)$ are obtained from the Fourier transformation of $\tilde{\phi}_B^\pm(t, \mu)$. The static B -meson decay constant $\tilde{f}_B(\mu)$ can be further expressed in terms of the QCD decay constant

$$\tilde{f}_B(\mu) = \left\{ 1 - \frac{\alpha_s(\mu) C_F}{4\pi} \left[3 \ln \frac{\mu}{m_b} + 2 \right] \right\}^{-1} f_B. \quad (6)$$

Employing the standard definitions for the decay constant of the D -meson and for $B \rightarrow D$ transition form factors

$$\begin{aligned} \langle D(p) | \bar{c} \gamma_\mu b | \bar{B}(p_B) \rangle &= f_{BD}^+(q^2) \left[2 p_\mu + \left(1 - \frac{m_B^2 - m_D^2}{q^2} \right) q_\mu \right] + f_{BD}^0(q^2) \frac{m_B^2 - m_D^2}{q^2} q_\mu, \\ \langle 0 | \bar{q} \not{n} \gamma_5 u | D(p) \rangle &= i n \cdot p f_D, \end{aligned} \quad (7)$$

it is straightforward to write down the hadronic dispersion relation for the correlation function

$$\begin{aligned} \Pi_\mu(n \cdot p, \bar{n} \cdot p) = & \frac{i f_D m_B}{2(m_D^2/n \cdot p - \bar{n} \cdot p)} \left\{ \bar{n}_\mu \left[\frac{n \cdot p}{m_B} f_{BD}^+(q^2) + f_{BD}^0(q^2) \right] \right. \\ & \left. + n_\mu \frac{m_B}{n \cdot p - m_B} \left[\frac{n \cdot p}{m_B} f_{BD}^+(q^2) - f_{BD}^0(q^2) \right] \right\} \\ & + \int_{\omega_s}^{+\infty} d\omega' \frac{1}{\omega' - \bar{n} \cdot p - i0} [\rho^h(\omega', n \cdot p) n_\mu + \tilde{\rho}^h(\omega', n \cdot p) \bar{n}_\mu], \quad (8) \end{aligned}$$

at leading power in Λ/m_b , where ω_s is the effective threshold parameter for the D -meson channel. Applying the parton-hadron duality approximation for the hadronic dispersion integral and performing the Borel transformation with respect to the variable $\bar{n} \cdot p$ lead to the LCSR for the two $B \rightarrow D$ form factors at tree level

$$\begin{aligned} f_{BD, 2P}^+(q^2) &= \frac{\tilde{f}_B(\mu) m_B}{f_D n \cdot p} \text{Exp} \left[\frac{m_D^2}{n \cdot p \omega_M} \right] \int_0^{\omega_s - \omega_c} d\omega' \text{Exp} \left[-\frac{\omega' + \omega_c}{\omega_M} \right] \phi_B^-(\omega') + \mathcal{O}(\alpha_s), \\ f_{BD, 2P}^0(q^2) &= \frac{n \cdot p}{m_B} f_{BD, 2P}^+(q^2) + \mathcal{O}(\alpha_s), \quad (9) \end{aligned}$$

where the upper limit of the ω' -integration is consistent with $\omega_0(q^2, s_0^D)$ derived in [10] at leading power in Λ/m_b keeping in mind the replacement rule $s_D \rightarrow n \cdot p \omega_s$. In contrast to the sum rules for $B \rightarrow \pi$ form factors, the power counting rule of ω_s and ω_M now reads

$$\omega_s \sim \omega_M \sim \mathcal{O}(\Lambda), \quad (10)$$

due to the scaling law $m_c^2 \sim m_D^2 \sim \mathcal{O}(m_b \Lambda)$. Based upon the canonical behaviour for the B -meson DA $\phi_B^-(\omega')$, one can readily deduce the power counting of $f_{BD}^+(q^2)$ at large hadronic recoil as $\mathcal{O}(\sqrt{\Lambda/m_b})$ from the tree-level sum rules (9), different from the scaling law $f_{BD}^+(q^2) \sim \mathcal{O}(1)$ [14] obtained with the counting scheme $m_c \sim m_b$. In addition, the two form factors $f_{BD}^{+,0}(q^2)$ obtained in the above respect the large-energy symmetry relation as discussed in [35] and the symmetry breaking effects can arise from both perturbative QCD corrections to the short-distance coefficient functions and the subleading power contributions from the higher-twist DA of the B -meson.

3 Two-particle contributions to the LCSR at $\mathcal{O}(\alpha_s)$

The purpose of this section is to demonstrate QCD factorization for the two-particle contribution to the vacuum-to- B -meson correlation function (1)

$$\begin{aligned} \Pi_{\mu, 2P}(n \cdot p, \bar{n} \cdot p) = & -i \tilde{f}_B(\mu) m_B \sum_{i=\pm} \int_0^\infty \frac{d\omega}{\bar{n} \cdot p - \omega - \omega_c + i0} \\ & \left[C_{i,n}(n \cdot p) J_{i,n}(\bar{n} \cdot p, \omega) n_\mu + C_{i,\bar{n}}(n \cdot p) J_{i,\bar{n}}(\bar{n} \cdot p, \omega) \bar{n}_\mu \right] \phi_B^i(\omega), \quad (11) \end{aligned}$$

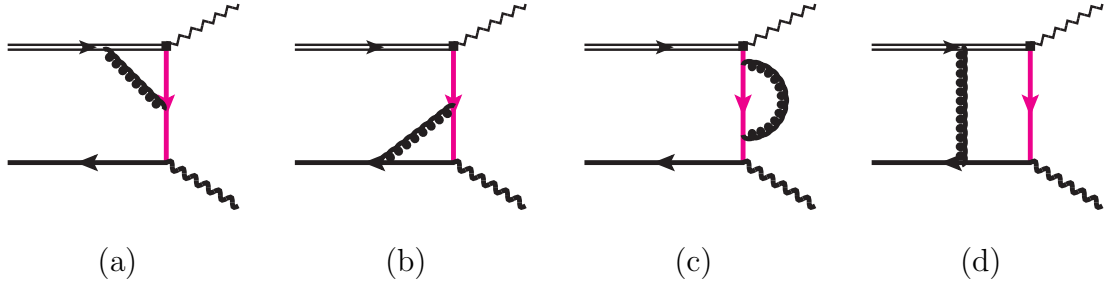


Figure 2: Diagrammatical representation of the two-particle contribution to the vacuum-to- B -meson correlation function $\Pi_\mu(n \cdot p, \bar{n} \cdot p)$ defined in (1) at $\mathcal{O}(\alpha_s)$.

at leading power in HQE. We will compute the hard matching coefficients $C_{i,k}$ ($i = \pm$, $k = n$ or \bar{n}) and the jet functions $J_{i,k}$ at next-to-leading order (NLO) in α_s manifestly applying the method of regions and perform QCD resummation for the large logarithms in the short-distance functions at NLL accuracy with the RG evolution in momentum space. Since the perturbative matching coefficients must be independent of the external partonic states in the OPE calculation, we will choose the initial state to be of the minimal quark and gluon degrees of freedom $|b(p_b) \bar{q}(k)\rangle$ for the convenience.

3.1 Perturbative matching functions at NLO

The NLO hard and jet functions entering the factorization formula (11) can be extracted by computing the leading power contributions of the one-loop QCD diagrams displayed in figure 2 from the hard and hard-collinear regions. It is evident that the soft contributions to the above-mentioned QCD diagrams at leading power in Λ/m_b will be cancelled out precisely by the infrared subtraction terms following the presentation [15] and we will mainly focus on the hard and hard-collinear contributions of the one-loop diagrams in figure 2 in the following.

3.1.1 Weak vertex diagram

We are now ready to compute the one-loop correction to the weak vertex diagram displayed in figure 2 (a)

$$\Pi_{\mu, \text{weak}}^{(1)} = \frac{i g_s^2 C_F}{(p - k)^2 - m_c^2 + i0} \int \frac{d^D l}{(2\pi)^D} \frac{1}{[(p - k + l)^2 - m_c^2 + i0][(m_b v + l)^2 - m_b^2 + i0][l^2 + i0]} \bar{q}(k) \not{v} \gamma_5 (\not{p} - \not{k} + m_c) \gamma_\rho (\not{p} - \not{k} + \not{l} + m_c) \gamma_\mu (m_b \not{v} + \not{l} + m_b) \gamma^\rho b(v), \quad (12)$$

where the external bottom and light quarks are taken to be on the mass-shell with the momenta $m_b v$ and k (with $k^2 = 0$). Employing the power counting scheme for the external momenta

$$n \cdot p \sim \mathcal{O}(m_b) \quad \bar{n} \cdot p \sim \mathcal{O}(\Lambda) \quad k \sim \mathcal{O}(\Lambda), \quad (13)$$

it is straightforward to identify that the leading power contributions to the scalar integral

$$I_1 = \int \frac{d^D l}{(2\pi)^D} \frac{1}{[(p - k + l)^2 - m_c^2 + i0][(m_b v + l)^2 - m_b^2 + i0][l^2 + i0]} \quad (14)$$

come from the hard, hard-collinear and soft regions of the loop momentum. Evaluating the hard contribution from the weak vertex diagram with the method of regions yields

$$\begin{aligned} \Pi_{\mu, \text{weak}}^{(1), h} &= \frac{i g_s^2 C_F}{\bar{n} \cdot p - \bar{n} \cdot k - \omega_c} \int \frac{d^D l}{(2\pi)^D} \frac{1}{[l^2 + n \cdot p \bar{n} \cdot l + i0][l^2 + 2m_b v \cdot l + i0][l^2 + i0]} \\ &\times \left\{ \bar{n}_\mu [2m_b n \cdot (p + l) + (D - 2) l_\perp^2] - n_\mu (D - 2) (\bar{n} \cdot l)^2 \right\} \bar{q}(k) \not{h} \gamma_5 b(v) \\ &= -\frac{1}{\bar{n} \cdot p - \bar{n} \cdot k - \omega_c} \left[\bar{n}_\mu C_{h, \bar{n}}^{(\text{weak})}(n \cdot p) + n_\mu C_{h, n}^{(\text{weak})}(n \cdot p) \right] \bar{q}(k) \not{h} \gamma_5 b(v), \end{aligned} \quad (15)$$

where we have introduced the following conventions

$$l_\perp^2 \equiv g_\perp^{\mu\nu} l_\mu l_\nu, \quad g_\perp^{\mu\nu} \equiv g^{\mu\nu} - \frac{n^\mu \bar{n}^\nu}{2} - \frac{n^\nu \bar{n}^\mu}{2}. \quad (16)$$

Computing the loop integrals with the expressions collected in Appendix A of [15], we obtain

$$\begin{aligned} C_{h, \bar{n}}^{(\text{weak})}(n \cdot p) &= -\frac{\alpha_s C_F}{4\pi} \left[\frac{1}{\epsilon^2} + \frac{1}{\epsilon} \left(2 \ln \frac{\mu}{n \cdot p} + 1 \right) + 2 \ln^2 \frac{\mu}{n \cdot p} + 2 \ln \frac{\mu}{m_b} \right. \\ &\quad \left. - 2 \text{Li}_2 \left(1 - \frac{1}{r} \right) - \ln^2 r + \frac{2-r}{r-1} \ln r + \frac{\pi^2}{12} + 3 \right], \\ C_{h, n}^{(\text{weak})}(n \cdot p) &= -\frac{\alpha_s C_F}{4\pi} \left[\frac{1}{r-1} \left(1 + \frac{r}{1-r} \ln r \right) \right], \end{aligned} \quad (17)$$

with $r = n \cdot p / m_b$, which coincide with the hard functions for the counterpart correlation function with a pion interpolating current [15] as expected.

The hard-collinear contribution to the weak vertex diagram can be further computed by expanding (12), in the hard-collinear region, at leading power in Λ/m_b

$$\begin{aligned} \Pi_{\mu, \text{weak}}^{(1), hc} &= \frac{i g_s^2 C_F}{\bar{n} \cdot p - \bar{n} \cdot k - \omega_c} \int \frac{d^D l}{(2\pi)^D} \frac{2 n \cdot (p + l) \bar{n}_\mu}{[n \cdot (p + l) \bar{n} \cdot (p - k + l) + l_\perp^2 - m_c^2 + i0][n \cdot l + i0][l^2 + i0]} \\ &\times \bar{d}(k) \not{h} \gamma_5 b(v) \\ &= -\frac{1}{\bar{n} \cdot p - \bar{n} \cdot k - \omega_c} \left[\bar{n}_\mu J_{-, \bar{n}}^{(\text{weak})}(\bar{n} \cdot p) \right] \bar{q}(k) \not{h} \gamma_5 b(v). \end{aligned} \quad (18)$$

Applying the results of loop integrals presented in Appendix A leads to

$$J_{-, \bar{n}}^{(\text{weak})}(\bar{n} \cdot p) = \frac{\alpha_s C_F}{4\pi} \left\{ \frac{2}{\epsilon^2} + \frac{2}{\epsilon} \left[\ln \frac{\mu^2}{n \cdot p (\omega - \bar{n} \cdot p)} - \ln (1 + r_1) + 1 \right] + \ln^2 \frac{\mu^2}{n \cdot p (\omega - \bar{n} \cdot p)} \right\}$$

$$\begin{aligned}
& + 2 \ln \frac{\mu^2}{n \cdot p (\omega - \bar{n} \cdot p)} - 2 \ln(1 + r_1) \left[\ln \frac{\mu^2}{n \cdot p (\omega - \bar{n} \cdot p)} + 1 \right] + \ln^2(1 + r_1) \\
& + 2 r_1 \ln \left(\frac{r_1}{1 + r_1} \right) - 2 \text{Li}_2 \left(\frac{1}{1 + r_1} \right) + \frac{\pi^2}{6} + 4 \Big\} ,
\end{aligned} \tag{19}$$

with $r_1 = m_c^2 / [n \cdot p \bar{n} \cdot (k - p)]$ and $\omega \equiv \bar{n} \cdot k$. It is apparent that our result of $J_{-, \bar{n}}^{(\text{weak})}$ reproduces the hard-collinear contribution to the weak vertex diagram, displayed in (29) of [15], for constructing the sum rules of $B \rightarrow \pi$ form factors in the $m_c \rightarrow 0$ (namely, $r_1 \rightarrow 0$) limit.

Proceeding in a similar manner, we can extract the soft contribution to the weak vertex diagram by expanding (12) in the soft region

$$\begin{aligned}
\Pi_{\mu, \text{weak}}^{(1), s} = & \frac{i g_s^2 C_F}{\bar{n} \cdot p - \bar{n} \cdot k - \omega_c} \int \frac{d^D l}{(2\pi)^D} \frac{\bar{n}_\mu}{[\bar{n} \cdot (p - k + l) - \omega_c + i0][v \cdot l + i0][l^2 + i0]} \\
& \times \bar{q}(k) \not{h} \gamma_5 b(v) ,
\end{aligned} \tag{20}$$

which is precisely the same as the soft subtraction term defined by the convolution integral of the partonic DA of the B -meson at NLO in α_s , calculable from the Wilson-line Feynman rules, and the tree-level short-distance function (see [15] for more discussion). We are then led to conclude that the soft QCD dynamics of the weak vertex diagram is indeed characterized by the B -meson DA at leading power in Λ/m_b , independent of the renormalization scheme.

3.1.2 D -meson vertex diagram

We turn to compute the one-loop QCD correction to the D -meson vertex diagram displayed in figure 2(b)

$$\begin{aligned}
\Pi_{\mu, D}^{(1)} = & - \frac{i g_s^2 C_F}{n \cdot p (\bar{n} \cdot p - \omega - \omega_c)} \int \frac{d^D l}{(2\pi)^D} \frac{1}{[(p - l)^2 - m_c^2 + i0][(l - k)^2 + i0][l^2 + i0]} \\
& \bar{q}(k) \gamma_\rho \not{l} \not{h} \gamma_5 (\not{p} - \not{l} + m_c) \gamma^\rho (\not{p} - \not{k} + m_c) \gamma_\mu b(v) .
\end{aligned} \tag{21}$$

Inspecting the scalar integral and the Dirac algebra of (21) with the power counting scheme (13), one can verify that the leading power contributions to the D -meson vertex diagram only arise from the hard-collinear and soft regions of the loop momentum. As already discussed in [15], it turns out to be more apparent to compute the loop integrals directly and then to expand the obtained expression up to the leading power in Λ/m_b , instead of applying the strategy of regions. Employing the results of loop integrals collected in Appendix A and the light-cone projector of the B -meson in momentum space derived in [35, 36] yields

$$\begin{aligned}
\Pi_{\mu, D}^{(1)} = & - \frac{i \tilde{f}_B(\mu) m_B}{\bar{n} \cdot p - \omega - \omega_c} \left\{ \bar{n}_\mu \phi_B^-(\omega) J_{-, \bar{n}}^{(D)}(\bar{n} \cdot p) + n_\mu \phi_B^+(\omega) J_{+, \bar{n}}^{(D)}(\bar{n} \cdot p) \right. \\
& \left. - \frac{m_c}{\bar{n} \cdot p} \phi_B^+(\omega) \bar{n}_\mu J_{+, \bar{n}}^{(D)}(\bar{n} \cdot p) - \frac{2 m_c^2}{p^2} [\bar{n}_\mu \phi_B^-(\omega) + n_\mu \phi_B^+(\omega)] \delta J^{(D)}(\bar{n} \cdot p) \right\} ,
\end{aligned} \tag{22}$$

where we have introduced the following jet functions

$$\begin{aligned} J_{-, \bar{n}}^{(D)}(\bar{n} \cdot p) = & \frac{\alpha_s C_F}{4\pi} \left\{ \left[\frac{2(1+r_2)}{r_3} \ln \left(\frac{1+r_2+r_3}{1+r_2} \right) - 1 \right] \left[\frac{1}{\epsilon} + \ln \left(-\frac{\mu^2}{p^2} \right) \right] \right. \\ & - \frac{2(1+r_2)}{r_3} \left[\text{Li}_2 \left(\frac{1}{1+r_2} \right) - \text{Li}_2 \left(\frac{1+r_3}{1+r_2+r_3} \right) \right] + \ln(1+r_2) \\ & - \frac{1+r_2}{r_3} \ln \left(\frac{1+r_2+r_3}{1+r_2} \right) \left[\ln \left(\frac{1+r_2+r_3}{1+r_2} \right) - \frac{2(2+r_3)(1+r_2+r_3)}{(1+r_2)(1+r_3)} \right. \\ & \left. \left. + 2 \ln(1+r_2) \right] + \frac{r_2 [r_2(1+r_3)-2]}{1+r_3} \ln \left(\frac{1+r_2}{r_2} \right) - (4+r_2) \right\}, \end{aligned} \quad (23)$$

$$J_{+, \bar{n}}^{(D)}(\bar{n} \cdot p) = \frac{\alpha_s C_F}{4\pi} \left\{ \frac{(1+r_3)^2 - r_2^2}{r_3(1+r_3)} \ln \left(\frac{1+r_2+r_3}{1+r_2} \right) + \frac{r_2^2(2+r_3)}{1+r_3} \ln \left(\frac{1+r_2}{r_2} \right) - r_2 \right\}, \quad (24)$$

$$\begin{aligned} J_{+, \bar{n}}^{(D)}(\bar{n} \cdot p) = & \frac{\alpha_s C_F}{4\pi} \left\{ \frac{(1+r_2+r_3)^2}{r_3(1+r_3)^2} \ln \left(\frac{1+r_2+r_3}{1+r_2} \right) + \frac{r_2}{1+r_3} \right. \\ & \left. - \frac{r_2 [2(1+r_3) + r_2(2+r_3)]}{(1+r_3)^2} \ln \left(\frac{1+r_2}{r_2} \right) \right\}, \end{aligned} \quad (25)$$

$$\delta J^{(D)}(\bar{n} \cdot p) = \frac{\alpha_s C_F}{4\pi} \left\{ \frac{1+r_2+r_3}{r_3(1+r_3)} \ln(1+r_2+r_3) - \frac{1+r_2}{r_3} \ln(1+r_2) + \frac{r_2}{1+r_3} \ln r_2 \right\}, \quad (26)$$

with

$$r_2 = -\frac{m_c^2}{p^2}, \quad r_3 = -\frac{\bar{n} \cdot k}{\bar{n} \cdot p}. \quad (27)$$

Several remarks on the resulting expressions for the QCD correction to the D -meson vertex diagram presented in (22) are in order.

- It is evident that the linear term in the charm-quark mass corresponds to the power enhanced effect compared to the remaining contributions due to the power counting scheme $m_c \sim \mathcal{O}(\sqrt{\Lambda m_b})$ and $\bar{n} \cdot p \sim \mathcal{O}(\Lambda)$. This observation can be readily understood from the fact that the SU(3) flavour symmetry breaking effect for heavy-to-light form factors (e.g., $B \rightarrow \pi$ and $B \rightarrow K$ transitions) is suppressed by m_s/Λ , but not power of m_s/m_b , compared to the leading power contribution in HQE [17], and the charm-quark mass effect would naturally induce flavour symmetry violation between $B \rightarrow D$ and $B \rightarrow \pi$ form factors with a scaling factor of $m_c/\Lambda \sim \mathcal{O}(\sqrt{m_b/\Lambda})$ in light of our power counting scheme. As there is no power enhanced contribution proportional to the charm-quark mass at tree level, the NLO jet function $J_{+, \bar{n}}^{(D)}(\bar{n} \cdot p)$ must be infrared finite to validate the factorization formula (11) for the considered correlation function.
- Setting $m_c \rightarrow 0$ (namely $r_2 \rightarrow 0$), our results of $J_{-, \bar{n}}^{(D)}(\bar{n} \cdot p)$ and $J_{+, \bar{n}}^{(D)}(\bar{n} \cdot p)$ will be reduced to the corresponding hard-collinear contributions from the pion vertex diagram as displayed in (38) of [15].

- Applying the Wilson-line Feynman rules, one can easily verify that the soft contribution to the D -meson vertex diagram, at leading power in Λ/m_b , is cancelled out precisely by the corresponding soft subtraction term.

3.1.3 Wave function renormalization

We proceed to compute the self-energy correction to the intermediate charm-quark propagator shown in figure 2(c). With the expressions of loop integrals collected in Appendix A, we obtain

$$\Pi_{\mu, wfc}^{(1)} = -\frac{1}{\bar{n} \cdot p - \bar{n} \cdot k - \omega_c} \left[\bar{n}_\mu J_{-, \bar{n}}^{(wfc)}(\bar{n} \cdot p) \right] \bar{q}(k) \not{h} \gamma_5 b(v), \quad (28)$$

which is apparently free of soft and collinear divergences. The resulting jet function reads

$$J_{-, \bar{n}}^{(wfc)}(\bar{n} \cdot p) = \frac{\alpha_s C_F}{4\pi} \left[J_{-, \bar{n}}^{(wfc, 1)}(\bar{n} \cdot p) - \frac{2r_1}{1+r_1} J_{-, \bar{n}}^{(wfc, 2)}(\bar{n} \cdot p) \right], \quad (29)$$

$$J_{-, \bar{n}}^{(wfc, 1)}(\bar{n} \cdot p) = -\left\{ \frac{1}{\epsilon} + \ln \left(-\frac{\mu^2}{(p-k)^2} \right) + r_1^2 \ln \left(\frac{1+r_1}{r_1} \right) - \ln(1+r_1) + 1 - r_1 \right\}, \quad (30)$$

$$J_{-, \bar{n}}^{(wfc, 2)}(\bar{n} \cdot p) = \frac{3}{\epsilon} + 3 \ln \left(-\frac{\mu^2}{(p-k)^2} \right) - r_1 (r_1 + 4) \ln \left(\frac{1+r_1}{r_1} \right) - 3 \ln(1+r_1) + r_1 + 5, \quad (31)$$

where the ultraviolet divergence of $J_{-, \bar{n}}^{(wfc, 2)}$ will be subtracted after the charm-quark mass renormalization dependent on the subtraction scheme. We will employ the $\overline{\text{MS}}$ renormalization scheme for the charm-loop mass, which is appropriate for a Lagrange parameter entering the short-distance matching function in the OPE calculation, and more discussion on the renormalization schemes of the charm-quark mass can be found in [12].

It is straightforward to compute the matching coefficients from the wave function renormalization of the external quarks

$$\Pi_{\mu, bwf}^{(1)} - \Phi_{b\bar{q}, bwf}^{(1)} \otimes T_\mu^{(0)} = -\frac{1}{\bar{n} \cdot p - \bar{n} \cdot k - \omega_c} \left[\bar{n}_\mu C_{-, \bar{n}}^{(bwf)}(n \cdot p) \right] \bar{q}(k) \not{h} \gamma_5 b(v), \quad (32)$$

$$\Pi_{\mu, qwf}^{(1)} - \Phi_{b\bar{q}, qwf}^{(1)} \otimes T_\mu^{(0)} = 0, \quad (33)$$

where $\Phi_{b\bar{q}}$ indicates the partonic DA of the B -meson defined in (12) of [15], the tree-level hard kernel $T_\mu^{(0)}$ can be readily deduced from (3) and the explicit expression of $C_{-, \bar{n}}^{(bwf)}$ is given by

$$C_{-, \bar{n}}^{(bwf)}(n \cdot p) = -\frac{\alpha_s C_F}{8\pi} \left[\frac{3}{\epsilon} + 3 \ln \frac{\mu^2}{m_b^2} + 4 \right]. \quad (34)$$

3.1.4 Box diagram

The one-loop QCD correction to the box diagram displayed in figure 2(d) can be further computed as

$$\Pi_{\mu, box}^{(1)} = -i g_s^2 C_F \int \frac{d^D l}{(2\pi)^D} \frac{1}{[(p_b + l)^2 - m_b^2 + i0][(p - k + l)^2 - m_c^2 + i0][(k - l)^2 + i0][l^2 + i0]}$$

$$\bar{q}(k) \gamma_\rho (k - l) \not{h} \gamma_5 (\not{p} - k + l + m_c) \gamma_\mu (\not{p}_b + l + m_b) \gamma^\rho b(v). \quad (35)$$

Taking advantage of the power counting scheme (13), one can identify that the leading power contributions to the box diagram come from the hard-collinear and soft regions of the loop momentum. Expanding the QCD expression of the box diagram (35) in the hard-collinear region to the leading power in Λ/m_b yields

$$\begin{aligned} \Pi_{\mu, box}^{(1), hc} = & -\frac{i g_s^2 C_F}{m_b} \int \frac{d^D l}{(2\pi)^D} \bar{q}(k) [(D-2) n \cdot l \not{h} - 2 m_b \not{h}] \gamma_5 b(v) \\ & \times \frac{n \cdot (p+l) \bar{n}_\mu}{[n \cdot (p+l) \bar{n} \cdot (p-k+l) + l_\perp^2 - m_c^2 + i0][n \cdot l \bar{n}(l-k) + l_\perp^2 + i0][l^2 + i0]} \end{aligned} \quad (36)$$

Employing the results of loop integrals collected in Appendix A and the momentum-space projector of the B -meson leads to

$$\Pi_{\mu, box}^{(1), hc} = -\frac{i \tilde{f}_B(\mu) m_B}{\bar{n} \cdot p - \omega - \omega_c} \bar{n}_\mu \left\{ \phi_B^-(\omega) J_{-, \bar{n}}^{(box)}(\bar{n} \cdot p) + \phi_B^+(\omega) J_{+, \bar{n}}^{(box)}(\bar{n} \cdot p) \right\}, \quad (37)$$

$$\begin{aligned} J_{-, \bar{n}}^{(box)} = & \frac{\alpha_s C_F}{2\pi} \frac{(1+r_1)(1+r_3)}{r_3} \left\{ \ln \left(1 - \frac{r_4}{1+r_1} \right) \left[\frac{1}{\epsilon} + \ln \left(\frac{\mu^2}{n \cdot p (\omega - \bar{n} \cdot p)} \right) \right. \right. \\ & - \frac{1}{2} \ln \left(1 - \frac{r_4}{1+r_1} \right) - \ln(1+r_1) + 1 + \frac{r_1}{1-r_4} \Big] + \text{Li}_2 \left(1 - \frac{r_1}{1+r_1-r_4} \right) \\ & \left. \left. - \text{Li}_2 \left(\frac{1}{1+r_1} \right) - \frac{r_1 r_4}{1-r_4} \ln \left(\frac{r_1}{1+r_1} \right) \right\}, \right. \end{aligned} \quad (38)$$

$$\begin{aligned} J_{+, \bar{n}}^{(box)} = & \frac{\alpha_s C_F}{4\pi} \frac{(1+r_1)(1+r_3)}{r_3} r \left\{ \left(\frac{r_1^2}{(1-r_4)^2} - 1 \right) \ln(1-r_4+r_1) - \frac{r_1 r_4}{1-r_4} \right. \\ & \left. + (1-r_1^2) \ln(1+r_1) - \frac{r_1^2 r_4 (2-r_4)}{(1-r_4)^2} \ln r_1 \right\}, \end{aligned} \quad (39)$$

where $r_4 = r_3/(1+r_3)$ with r_3 defined in (27). One can readily verify that the resulting jet functions $J_{-, \bar{n}}^{(box)}$ and $J_{+, \bar{n}}^{(box)}$ reproduce the hard-collinear contribution to the one-loop box diagram for the vacuum-to- B -meson correlation function with a pion interpolating current as presented in (52) of [15], in the $m_c \rightarrow 0$ limit.

The soft contribution to the one-loop box diagram at leading power in Λ/m_b can be further extracted from (35) with the method of regions

$$\begin{aligned} \Pi_{\mu, box}^{(1), s} = & -\frac{g_s^2 C_F}{2} \int \frac{d^D l}{(2\pi)^D} \frac{1}{[v \cdot l + i0][\bar{n} \cdot (p-k+l) - \omega_c + i0][(k-l)^2 + i0][l^2 + i0]} \\ & \bar{q}(k) \not{p} (k - l) \not{h} \gamma_5 \not{h} \gamma_\mu b(v), \end{aligned} \quad (40)$$

which is precisely the same as the soft subtraction term $\Phi_{b\bar{q}, box}^{(1)} \otimes T_\mu^{(0)}$ computed with the Wilson-line Feynman rules. We then conclude that the soft dynamics of the vacuum-to- B -meson correlation function under discussion is indeed parameterized by the light-cone DA of the B -meson in HQET.

3.1.5 The NLL hard and jet functions

Now we are in a position to present the one-loop hard and jet functions entering the factorization formula (11) with resummation of the large logarithms by solving the corresponding RG equations in momentum space. Putting different pieces together, we first derive the renormalized hard coefficients including the $\mathcal{O}(\alpha_s)$ corrections

$$\begin{aligned} C_{+,n} &= C_{+,\bar{n}} = 1, \quad C_{-,n} = C_{h,n}^{(weak)} = -\frac{\alpha_s C_F}{4\pi} \left[\frac{1}{r-1} \left(1 + \frac{r}{1-r} \ln r \right) \right], \\ C_{-,\bar{n}} &= 1 + C_{h,\bar{n}}^{(weak)} + \left[\Pi_{\mu,bwf}^{(1)} - \Phi_{b\bar{q},bwf}^{(1)} \otimes T_\mu^{(0)} \right] \\ &= 1 - \frac{\alpha_s C_F}{4\pi} \left[2 \ln^2 \frac{\mu}{n \cdot p} + 5 \ln \frac{\mu}{m_b} - 2 \text{Li}_2 \left(1 - \frac{1}{r} \right) - \ln^2 r + \frac{2-r}{r-1} \ln r \right. \\ &\quad \left. + \frac{\pi^2}{12} + 5 \right], \end{aligned} \quad (41)$$

and the renormalized jet functions at one-loop accuracy are given by

$$\begin{aligned} J_{+,n} &= J_{+,n}^{(D)} - \frac{2m_c^2}{p^2} \delta J^{(D)} \\ &= \frac{\alpha_s C_F}{4\pi} \left\{ \frac{(1+r_2+r_3)^2}{r_3(1+r_3)} \ln \left(\frac{1+r_2+r_3}{1+r_2} \right) + \frac{r_2}{1+r_3} \left[r_2 r_3 \ln \left(\frac{1+r_2}{r_2} \right) - r_3 - 1 \right] \right\}, \end{aligned} \quad (42)$$

$$\begin{aligned} J_{+,\bar{n}} &= -\frac{m_c}{\bar{n} \cdot p} J_{+,\bar{n}}^{(D)} + J_{+,\bar{n}}^{(box)} \\ &= \frac{\alpha_s C_F}{4\pi} \left\{ -\frac{m_c}{\bar{n} \cdot p} \left[\frac{(1+r_2+r_3)^2}{r_3(1+r_3)^2} \ln \left(\frac{1+r_2+r_3}{1+r_2} \right) + \frac{r_2}{1+r_3} \right. \right. \\ &\quad \left. \left. - \frac{r_2 [2(1+r_3) + r_2(2+r_3)]}{(1+r_3)^2} \ln \left(\frac{1+r_2}{r_2} \right) \right] + \frac{r(1+r_2+r_3)}{(1+r_3)^2} \right. \\ &\quad \times \left. \left[\frac{(1+r_3)^2 - r_2^2}{r_3} \ln \left(\frac{1+r_2+r_3}{1+r_2} \right) + r_2^2(r_3+2) \ln \left(\frac{1+r_2}{r_2} \right) - r_2(1+r_3) \right] \right\}, \end{aligned} \quad (43)$$

$$J_{-,n} = 1, \quad (44)$$

$$\begin{aligned} J_{-,\bar{n}} &= 1 + \left[J_{-,\bar{n}}^{(weak)} + J_{-,\bar{n}}^{(D)} - \frac{2m_c^2}{p^2} \delta J^{(D)} + J_{-,\bar{n}}^{(wfc)} + J_{-,\bar{n}}^{(box)} \right] \\ &= 1 + \frac{\alpha_s C_F}{4\pi} \left\{ \ln^2 \left(\frac{\mu^2}{n \cdot p (\omega - \bar{n} \cdot p)} \right) - 2 \left[\ln \left(\frac{(1+r_2+r_3)^2}{(1+r_2)(1+r_3)} \right) + \frac{3r_2}{1+r_2+r_3} \right] \right. \\ &\quad \times \ln \left(\frac{\mu^2}{n \cdot p (\omega - \bar{n} \cdot p)} \right) + 2 \ln^2(1+r_2+r_3) - 4 \ln(1+r_2+r_3) \ln(1+r_3) \\ &\quad \left. + \ln^2(1+r_3) + \left[\frac{2(1+r_2)}{r_3} + \frac{r_2(r_2+2(1+r_3))}{(1+r_3)^2} - 1 \right] \ln(1+r_2+r_3) \right\} \end{aligned}$$

$$\begin{aligned}
& +2 \left[\ln(1+r_2) - \frac{3r_2}{1+r_2+r_3} \right] \ln(1+r_3) + \frac{(1+r_2)(r_3(1+r_2)-2)}{r_3} \ln(1+r_2) \\
& - \ln^2(1+r_2) + r_2 \left[\frac{6}{1+r_2+r_3} - \frac{r_2}{(1+r_3)^2} - \frac{2}{1+r_3} - r_2 - 2 \right] \ln r_2 + \frac{\pi^2}{6} - 1 \\
& - 4 \text{Li}_2\left(\frac{1+r_3}{1+r_2+r_3}\right) + 2 \text{Li}_2\left(\frac{1}{1+r_2}\right) - r_2 \left[\frac{8}{1+r_2+r_3} + \frac{1}{1+r_3} + 1 \right] \Big\}. \tag{45}
\end{aligned}$$

It is apparent that the hard functions $C_{-,n}$ and $C_{-,\bar{n}}$ are identical to the perturbative matching coefficients of the weak current $\bar{q} \gamma_\mu (1 - \gamma_5) b$ from QCD onto SCET, as discussed in [15], due to the power counting rule of the charm-quark mass displayed in (2). However, the hard-collinear functions entering the factorization formula (11) turn out to be significantly more involved, due to the massive charm-quark effect, than the counterpart jet functions for the massless hard-collinear quark.

To verify the factorization-scale independence of the correlation function Π_μ at $\mathcal{O}(\alpha_s)$, we make use of the RG evolution equation of the charm-quark mass [37, 38]

$$\frac{d \ln m_c(\mu)}{d \ln \mu} = - \sum_{n=0} \left(\frac{\alpha_s(\mu)}{4\pi} \right)^{n+1} \gamma_m^{(n)}, \quad \gamma_m^{(0)} = 6 C_F, \tag{46}$$

it is then straightforward to write down

$$\begin{aligned}
\frac{d}{d \ln \mu} \Pi_{\mu, 2P}(n \cdot p, \bar{n} \cdot p) &= -i \tilde{f}_B(\mu) m_B \frac{\alpha_s C_F}{4\pi} \int_0^\infty d\omega \frac{\phi_B^-(\omega, \mu)}{\bar{n} \cdot p - \omega - \omega_c - i0} \\
&\times \left\{ \frac{12r_2}{1+r_2+r_3} + 4 \left[\ln \left(\frac{\mu^2}{n \cdot p (\omega - \bar{n} \cdot p)} \right) - \ln \left(\frac{(1+r_2+r_3)^2}{(1+r_2)(1+r_3)} \right) - \frac{3r_2}{1+r_2+r_3} \right] \right. \\
&\left. - \left[4 \ln \left(\frac{\mu}{n \cdot p} \right) + 5 \right] \right\} - i m_B \int_0^\infty \frac{d\omega}{\bar{n} \cdot p - \omega - \omega_c - i0} \frac{d}{d \ln \mu} [\tilde{f}_B(\mu) \phi_B^-(\omega, \mu)], \tag{47}
\end{aligned}$$

where the three terms in the bracket arise from the RG running of the charm-quark mass, the jet function $J_{-,\bar{n}}$ and the hard function $C_{-,\bar{n}}$, respectively. Applying the one-loop evolution equation of the B -meson DA $\phi_B^-(\omega, \mu)$ in the absence of the light-quark mass effect [39, 40]

$$\frac{d}{d \ln \mu} [\tilde{f}_B(\mu) \phi_B^-(\omega, \mu)] = -\frac{\alpha_s C_F}{4\pi} \int_0^\infty d\omega' \mathcal{H}_-^{(1)}(\omega, \omega', \mu) [\tilde{f}_B(\mu) \phi_B^-(\omega', \mu)], \tag{48}$$

where the renormalization kernel is given by

$$\mathcal{H}_-^{(1)}(\omega, \omega', \mu) = \left[4 \ln \frac{\mu}{\omega} - 5 \right] \delta(\omega - \omega') - 4 \frac{\theta(\omega - \omega')}{\omega'} - 4\omega \left[\frac{\theta(\omega' - \omega)}{\omega'(\omega' - \omega)} + \frac{\theta(\omega - \omega')}{\omega(\omega - \omega')} \right]_{\oplus}, \tag{49}$$

with the \oplus function defined as follows

$$\int_0^\infty d\omega' [f(\omega, \omega')]_{\oplus} g(\omega') = \int_0^\infty d\omega' f(\omega, \omega') [g(\omega') - g(\omega)], \tag{49}$$

we can readily compute the last term of (47) as

$$\begin{aligned} & -i m_B \int_0^\infty \frac{d\omega}{\bar{n} \cdot p - \omega - \omega_c - i0} \frac{d}{d \ln \mu} \left[\tilde{f}_B(\mu) \phi_B^-(\omega, \mu) \right] \\ & = i \tilde{f}_B(\mu) m_B \frac{\alpha_s C_F}{4\pi} \int_0^\infty d\omega \frac{\phi_B^-(\omega, \mu)}{\bar{n} \cdot p - \omega - \omega_c - i0} \left[4 \ln \left(\frac{\mu}{\omega} \right) - 4 \ln \left(\frac{(1+r_2+r_3)^2}{(1+r_2)r_3} \right) - 5 \right]. \end{aligned} \quad (50)$$

Substituting (50) into (47) immediately leads to

$$\frac{d}{d \ln \mu} \Pi_{\mu, 2P}(n \cdot p, \bar{n} \cdot p) = \mathcal{O}(\alpha_s^2), \quad (51)$$

indicating that the correlation function computed from the factorization formula (11) is indeed independent of the renormalization scale to the one-loop accuracy.

We will proceed to perform the summation of parametrically large logarithms in the perturbative expansion of the short-distance functions at NLL applying the RG equations for the hard matching coefficients in momentum space. Following the arguments of [41], we will not aim at summing over logarithms of μ/μ_0 , with μ_0 being a hadronic scale of $\mathcal{O}(\Lambda)$, from the RG evolution of the B -meson DA $\phi_B^-(\omega, \mu)$, since we will take the factorization scale μ as a hard-collinear scale $\mu_{hc} \sim \mathcal{O}(\sqrt{\Lambda m_b})$ which is quite close to the hadronic scale μ_0 numerically. Employing the RG equations for the hard coefficient $C_{-, \bar{n}}(n \cdot p, \mu)$ and the static B -meson decay constant $\tilde{f}_B(\mu)$

$$\begin{aligned} \frac{dC_{-, \bar{n}}(n \cdot p, \mu)}{d \ln \mu} &= \left[-\Gamma_{\text{cusp}}(\alpha_s) \ln \frac{\mu}{n \cdot p} + \gamma(\alpha_s) \right] C_{-, \bar{n}}(n \cdot p, \mu), \\ \frac{d\tilde{f}_B(\mu)}{d \ln \mu} &= \tilde{\gamma}(\alpha_s) \tilde{f}_B(\mu), \end{aligned} \quad (52)$$

where the anomalous dimensions are expanded perturbatively in QCD

$$\begin{aligned} \Gamma_{\text{cusp}}(\alpha_s) &= \sum_{n=0} \left(\frac{\alpha_s}{4\pi} \right)^{n+1} \Gamma_{\text{cusp}}^{(n)}, \quad \gamma(\alpha_s) = \sum_{n=0} \left(\frac{\alpha_s}{4\pi} \right)^{n+1} \gamma^{(n)}, \\ \tilde{\gamma}(\alpha_s) &= \sum_{n=0} \left(\frac{\alpha_s}{4\pi} \right)^{n+1} \tilde{\gamma}^{(n)}. \end{aligned} \quad (53)$$

To achieve the resummation improved factorization formula for the considered correlation function at NLL accuracy, the cusp anomalous dimension $\Gamma_{\text{cusp}}(\alpha_s)$ needs to be expanded at the three-loop accuracy, while the soft anomalous dimensions $\gamma(\alpha_s)$ and $\tilde{\gamma}(\alpha_s)$ need to be expanded up to two loops. The NLL resummation improved expressions for $C_{-, \bar{n}}$ and \tilde{f}_B can be further computed as

$$\begin{aligned} C_{-, \bar{n}}(n \cdot p, \mu) &= U_1(n \cdot p, \mu_{h1}, \mu) C_{-, \bar{n}}(n \cdot p, \mu_{h1}), \\ \tilde{f}_B(\mu) &= U_2(n \cdot p, \mu_{h2}, \mu) \tilde{f}_B(\mu_{h2}), \end{aligned} \quad (54)$$

where the explicit expressions of the evolution functions U_1 and U_2 can be found in [20]. It is then a straightforward task to deduce the resummation improved factorization formula for the correlation function Π_μ

$$\begin{aligned} \Pi_{\mu, 2P}(n \cdot p, \bar{n} \cdot p) = & -i \left[U_2(n \cdot p, \mu_{h2}, \mu) \tilde{f}_B(\mu_{h2}) \right] m_B \int_0^\infty \frac{d\omega}{\bar{n} \cdot p - \omega - \omega_c + i0} \\ & \times \left\{ \left[C_{+,n}(n \cdot p, \mu) J_{+,n}(\bar{n} \cdot p, \omega, \mu) n_\mu + C_{+,\bar{n}}(n \cdot p, \mu) J_{+,\bar{n}}(\bar{n} \cdot p, \omega, \mu) \bar{n}_\mu \right] \phi_B^+(\omega, \mu) \right. \\ & + \left[C_{-,n}(n \cdot p, \mu) J_{-,n}(\bar{n} \cdot p, \omega, \mu) n_\mu + U_1(n \cdot p, \mu_{h1}, \mu) C_{-,\bar{n}}(n \cdot p, \mu_{h1}) J_{-,\bar{n}}(\bar{n} \cdot p, \omega, \mu) \bar{n}_\mu \right] \\ & \left. \times \phi_B^-(\omega, \mu) \right\}, \end{aligned} \quad (55)$$

where μ_{h1} and μ_{h2} are the hard scales of $\mathcal{O}(m_b)$ and the factorization scale μ needs to be taken at a hard-collinear scale $\mathcal{O}(\sqrt{m_b \Lambda})$.

3.2 The NLL LCSR for $B \rightarrow D$ form factors

We are now ready to derive the NLL resummation improved sum rules for the vector and scalar $B \rightarrow D$ form factors. To this end, it is mandatory to work out the spectral representation of the factorization formula for Π_μ obtained in the above, which turns out to be a nontrivial task compared to the construction of the B -meson LCSR for $B \rightarrow \pi$ form factors [15]. Applying the dispersion representations of convolution integrals collected in Appendix B yields

$$\begin{aligned} \Pi_{\mu, 2P}(n \cdot p, \bar{n} \cdot p) = & -i \left[U_2(n \cdot p, \mu_{h2}, \mu) \tilde{f}_B(\mu_{h2}) \right] m_B \int_0^\infty \frac{d\omega'}{\omega' - \bar{n} \cdot p - i0} \\ & \times \left\{ C_{+,n}(n \cdot p, \mu) \Phi_{+,n}^{\text{eff}}(\omega', \mu) n_\mu + C_{+,\bar{n}}(n \cdot p, \mu) \Phi_{+,\bar{n}}^{\text{eff}}(\omega', \mu) \bar{n}_\mu \right. \\ & + C_{-,n}(n \cdot p, \mu) \Phi_{-,n}^{\text{eff}}(\omega', \mu) n_\mu + U_1(n \cdot p, \mu_{h1}, \mu) C_{-,\bar{n}}(n \cdot p, \mu_{h1}) \Phi_{-,\bar{n}}^{\text{eff}}(\omega', \mu) \bar{n}_\mu \left. \right\}, \end{aligned} \quad (56)$$

where we have introduced the “effective” DA $\Phi_{i,k}^{\text{eff}}(\omega', \mu)$ ($i = \pm$, $k = n$ or \bar{n}) absorbing the hard-collinear QCD corrections to the correlation function

$$\begin{aligned} \Phi_{+,n}^{\text{eff}}(\omega', \mu) = & \frac{\alpha_s C_F}{4\pi} \left\{ \frac{\omega_c}{\omega'} \left[\frac{\omega' - \omega_c}{\omega'} \ln \left| \frac{\omega_c - \omega'}{\omega_c} \right| - 1 \right] \phi_B^+(\omega' - \omega_c) \theta(\omega' - \omega_c) \right. \\ & - \left[\omega_c \ln \left| \frac{\omega_c - \omega'}{\omega_c} \right| \delta'(\omega') - \delta(\omega') \right] \int_0^\infty d\omega \frac{\omega_c}{\omega + \omega_c} \phi_B^+(\omega) \\ & + \theta(\omega' - \omega_c) \int_0^\infty d\omega \left[\frac{\omega \omega_c}{(\omega + \omega_c)^2} \left(\mathcal{P} \frac{1}{\omega' - \omega - \omega_c} - \frac{1}{\omega'} \right) + \frac{\omega_c}{\omega} \frac{1}{\omega'} \right. \\ & \left. \left. + \frac{\omega_c^2}{\omega + \omega_c} \frac{1}{\omega'^2} - \frac{\theta(\omega + \omega_c - \omega')}{\omega} + \frac{\omega_c}{\omega} \frac{\theta(\omega' - \omega - \omega_c)}{\omega - \omega'} \right] \phi_B^+(\omega) \right\}, \end{aligned} \quad (57)$$

$$\begin{aligned}
\Phi_{+, \bar{n}}^{\text{eff}}(\omega', \mu) = & \frac{\alpha_s C_F}{4\pi} \left\{ m_c \left[\left(\frac{1}{\omega' - \omega_c} - \frac{1}{\omega'} - \frac{\omega_c - \omega'}{\omega'^2} \ln \left| \frac{\omega_c - \omega'}{\omega_c} \right| \right) \phi_B^+(\omega' - \omega_c) \theta(\omega' - \omega_c) \right. \right. \\
& + \frac{\omega_c}{\omega'} \theta(\omega' - \omega_c) \int_0^\infty d\omega \frac{d}{d\omega} \frac{\phi_B^+(\omega)}{\omega} - \left(\delta(\omega') - \omega_c \ln \left| \frac{\omega_c - \omega'}{\omega_c} \right| \delta'(\omega') \right) \\
& \times \int_0^\infty d\omega \frac{\omega_c}{\omega(\omega + \omega_c)} \phi_B^+(\omega) - \int_0^\infty d\omega \frac{\theta(\omega' - \omega - \omega_c)}{\omega' - \omega} \left(1 + \omega_c \frac{d}{d\omega} \right) \frac{\phi_B^+(\omega)}{\omega} \\
& + \theta(\omega' - \omega_c) \int_0^\infty d\omega \left(\frac{\omega}{(\omega + \omega_c)^2} \mathcal{P} \frac{1}{\omega' - \omega - \omega_c} + \frac{\omega_c(2\omega + \omega_c)}{\omega(\omega + \omega_c)^2} \frac{1}{\omega'} \right. \\
& \left. \left. - \frac{\omega_c^2}{\omega(\omega + \omega_c)} \frac{1}{\omega'^2} \right) \phi_B^+(\omega) \right] \\
& + r \left[\theta(\omega' - \omega_c) \frac{\omega_c^2}{\omega'^2} \int_0^\infty d\omega \left(1 - \omega' \frac{d}{d\omega} \right) \frac{\phi_B^+(\omega)}{\omega} \right. \\
& - \theta(\omega' - \omega_c) \int_0^\infty d\omega \theta(\omega + \omega_c - \omega') \left(1 - \omega_c \frac{d}{d\omega} \right) \frac{\phi_B^+(\omega)}{\omega} \\
& + \int_0^\infty d\omega \theta(\omega' - \omega - \omega_c) \frac{\omega_c^2}{\omega' - \omega} \frac{d}{d\omega} \frac{\phi_B^+(\omega)}{\omega} \\
& \left. \left. + \omega_c \left(\delta(\omega') - \omega_c \ln \left| \frac{\omega_c - \omega'}{\omega_c} \right| \delta'(\omega') \right) \int_0^\infty d\omega \frac{\phi_B^+(\omega)}{\omega} \right] \right\}, \tag{58}
\end{aligned}$$

$$\Phi_{-, n}^{\text{eff}}(\omega', \mu) = -\phi_B^-(\omega' - \omega_c) \theta(\omega' - \omega_c), \tag{59}$$

$$\begin{aligned}
\Phi_{-, \bar{n}}^{\text{eff}}(\omega', \mu) = & -\phi_B^-(\omega' - \omega_c) \theta(\omega' - \omega_c) + \frac{\alpha_s C_F}{4\pi} \left\{ \phi_B^-(\omega' - \omega_c) \theta(\omega' - \omega_c) \rho_{-, \bar{n}}^{(1)}(\omega') \right. \\
& + \left[\frac{d}{d\omega'} \phi_B^-(\omega' - \omega_c) \right] \theta(\omega' - \omega_c) \rho_{-, \bar{n}}^{(2)}(\omega') + \phi_B^-(\omega') \rho_{-, \bar{n}}^{(3)}(\omega') + \phi_B^-(0) \rho_{-, \bar{n}}^{(4)}(\omega') \\
& + \int_0^\infty d\omega \phi_B^-(\omega) \rho_{-, \bar{n}}^{(5)}(\omega, \omega') + \int_0^\infty d\omega \left[\frac{d}{d\omega} \phi_B^-(\omega) \right] \rho_{-, \bar{n}}^{(6)}(\omega, \omega') \\
& \left. + \int_0^\infty d\omega \left[\frac{d}{d\omega} \frac{\phi_B^-(\omega)}{\omega} \right] \rho_{-, \bar{n}}^{(7)}(\omega, \omega') \right\}, \tag{60}
\end{aligned}$$

with \mathcal{P} indicating the principle-value prescription. The tedious expressions of the coefficient functions $\rho_{-, \bar{n}}^{(i)}$ in (60) are collected in Appendix C. Applying the standard strategy to construct the sum rules for hadronic transition form factors by matching (56) and (8) with the aid of the parton-hadron duality approximation and the Borel transformation leads to

$$\begin{aligned}
f_D \text{Exp} \left[-\frac{m_D^2}{n \cdot p \omega_M} \right] \left\{ \frac{n \cdot p}{m_B} f_{BD, 2P}^+(q^2), f_{BD, 2P}^0(q^2) \right\} \\
= - \left[U_2(n \cdot p, \mu_{h2}, \mu) \tilde{f}_B(\mu_{h2}) \right] \int_0^{\omega_s} d\omega' \text{Exp} \left[-\frac{\omega'}{\omega_M} \right] \tag{61}
\end{aligned}$$

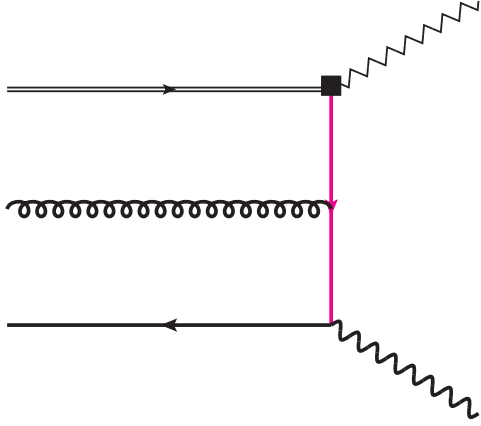


Figure 3: Diagrammatical representation of the three-particle contributions to the vacuum-to- B -meson correlation function $\Pi_\mu(n \cdot p, \bar{n} \cdot p)$ defined in (1) at tree level.

$$\times \left\{ C_{+, \bar{n}}(n \cdot p, \mu) \Phi_{+, \bar{n}}^{\text{eff}}(\omega', \mu) + U_1(n \cdot p, \mu_{h1}, \mu) C_{-, \bar{n}}(n \cdot p, \mu_{h1}) \Phi_{-, \bar{n}}^{\text{eff}}(\omega', \mu) \right. \\ \left. \pm \frac{n \cdot p - m_B}{m_B} [C_{+, n}(n \cdot p, \mu) \Phi_{+, n}^{\text{eff}}(\omega', \mu) + C_{-, n}(n \cdot p, \mu) \Phi_{-, n}^{\text{eff}}(\omega', \mu)] \right\}, \quad (62)$$

which serves as the master formula for the two-particle contributions to $B \rightarrow D$ form factors obtained in this paper. It is evident that the symmetry-breaking corrections to the form-factor relation (9) arise from both hard and hard-collinear fluctuations as displayed in the last line of (62), and the power enhanced contribution due to the charm-quark mass effect preserves the large-recoil symmetry relation.

4 Three-particle contributions to the LCSR at tree level

The objective of this section is to compute the tree-level contribution to the sum rules of $B \rightarrow D$ form factors from the three-particle B -meson DA. To this end, we first need to demonstrate QCD factorization for the three-particle contributions to the correlation function (1) with space-like interpolating momentum, which can be achieved by evaluating the diagram displayed in figure 3 with the aid of the light-cone OPE.

Employing the massive quark propagator near the light cone from the background gluon field method [42–44]

$$S(x, 0, m_c) = \langle 0 | T \{ \bar{c}(x), c(0) \} | 0 \rangle \\ \supset i \int_0^\infty \frac{d^4 k}{(2\pi)^4} e^{-ik \cdot x} \int_0^1 du \left[\frac{u x_\mu \gamma_\nu}{k^2 - m_c^2} - \frac{(k + m_c) \sigma_{\mu\nu}}{2(k^2 - m_c^2)^2} \right] G^{\mu\nu}(u x), \quad (63)$$

with $G^{\mu\nu} = g_s T^a G_{\mu\nu}^a$, it is then straightforward to derive the factorization formula

$$\begin{aligned}\Pi_{\mu,3P}(n \cdot p, \bar{n} \cdot p) = & -\frac{i \tilde{f}_B(\mu) m_B}{n \cdot p} \int_0^\infty d\omega \int_0^\infty d\xi \int_0^1 du \left\{ \frac{\tilde{\rho}_{2,n}(u, \omega, \xi)}{(\bar{n} \cdot p - \omega - u\xi - \omega_c)^2} n_\mu \right. \\ & \left. + \left[\frac{\tilde{\rho}_{2,\bar{n}}(u, \omega, \xi)}{(\bar{n} \cdot p - \omega - u\xi - \omega_c)^2} + \frac{\tilde{\rho}_{3,\bar{n}}(u, \omega, \xi)}{(\bar{n} \cdot p - \omega - u\xi - \omega_c)^3} \right] \bar{n}_\mu \right\},\end{aligned}\quad (64)$$

where the coefficient functions $\tilde{\rho}_{i,k}(u, \omega, \xi)$ are given by

$$\begin{aligned}\tilde{\rho}_{2,n}(u, \omega, \xi) &= 2(u-1) [\psi_V(\omega, \xi) + \psi_A(\omega, \xi)], \\ \tilde{\rho}_{2,\bar{n}}(u, \omega, \xi) &= -\psi_V(\omega, \xi) + (2u-1)\psi_A(\omega, \xi), \\ \tilde{\rho}_{3,\bar{n}}(u, \omega, \xi) &= 2(2u-1) [\bar{X}_A(\omega, \xi) - 2\bar{Y}_A(\omega, \xi)].\end{aligned}\quad (65)$$

The appeared three-particle DA of the B -meson can be defined by the position-space matrix element on the light cone [45, 46]

$$\begin{aligned}\langle 0 | \bar{q}_\alpha(x) G_{\lambda\rho}(ux) b_{v\beta}(0) | \bar{B}(v) \rangle|_{x^2=0} = & \frac{\tilde{f}_B(\mu) m_B}{4} \int_0^\infty d\omega \int_0^\infty d\xi e^{-i(\omega+u\xi)v \cdot x} \left[(1+\not{v}) \left\{ (v_\lambda \gamma_\rho - v_\rho \gamma_\lambda) [\Psi_A(\omega, \xi) - \Psi_V(\omega, \xi)] \right. \right. \\ & \left. \left. - i \sigma_{\lambda\rho} \Psi_V(\omega, \xi) - \frac{x_\lambda v_\rho - x_\rho v_\lambda}{v \cdot x} X_A(\omega, \xi) + \frac{x_\lambda \gamma_\rho - x_\rho \gamma_\lambda}{v \cdot x} Y_A(\omega, \xi) \right\} \gamma_5 \right]_{\beta\alpha},\end{aligned}\quad (66)$$

where we have neglected the soft Wilson lines to maintain the gauge invariance of the string operator on the left-hand side. The following conventions

$$\bar{X}_A(\omega, \xi) = \int_0^\omega d\eta X_A(\eta, \xi), \quad \bar{Y}_A(\omega, \xi) = \int_0^\omega d\eta Y_A(\eta, \xi), \quad (67)$$

are further introduced in (65) for convenience. Our current understanding of the model independent properties of the three-particle quark-gluon B -meson DA is limited to the twist-3 DA $\Phi_3(\omega, \xi) \equiv \Psi_A(\omega, \xi) - \Psi_V(\omega, \xi)$ which was shown to be completely integrable in the large N_c limit and to be solvable exactly at one loop [47]. Investigating perturbative QCD constraints on the higher-twist B -meson DA from the OPE analysis in the partonic picture and from the renormalization evolution equations in momentum (or “dual”) space, along the lines of [48, 49], would be interesting for the future work.

Expressing the factorization formula for the three-particle contributions to the correlation function $\Pi_{\mu,3P}$ in a dispersion form with respect to the variable $\bar{n} \cdot p$ and implementing the continuum subtraction with the aid of the parton-hadron duality relation as well as the Borel transformation lead to the following sum rules

$$f_D \text{Exp} \left[-\frac{m_D^2}{n \cdot p \omega_M} \right] \left\{ \frac{n \cdot p}{m_B} f_{BD,3P}^+(q^2), f_{BD,3P}^0(q^2) \right\}$$

$$= -\frac{\tilde{f}_B(\mu)}{n \cdot p} \left[\mathcal{F}_{3P,\bar{n}}(\omega_s, \omega_M) \mp \frac{m_B - n \cdot p}{m_B} \mathcal{F}_{3P,n}(\omega_s, \omega_M) \right], \quad (68)$$

where the explicit expressions of the coefficient functions $\mathcal{F}_{3P,\bar{n}}$ and $\mathcal{F}_{3P,n}$ are

$$\begin{aligned} \mathcal{F}_{3P,\bar{n}}(\omega_s, \omega_M) &= \int_0^{\omega_s - \omega_c} d\omega \int_{\omega_s - \omega_c - \omega}^{\infty} \frac{d\xi}{\xi} \text{Exp} \left(-\frac{\omega_s}{\omega_M} \right) \\ &\times \left[\tilde{\rho}_{2,\bar{n}}(u, \omega, \xi) - \frac{1}{2} \left(\frac{d}{d\omega} + \frac{1}{\omega_M} \right) \tilde{\rho}_{3,\bar{n}}(u, \omega, \xi) \right] \Big|_{u=\frac{\omega_s - \omega_c - \omega}{\xi}} \\ &+ \int_{\omega_c}^{\omega_s} d\omega' \int_0^{\omega' - \omega_c} d\omega \int_{\omega' - \omega_c - \omega}^{\infty} \frac{d\xi}{\xi} \frac{1}{\omega_M} \text{Exp} \left(-\frac{\omega'}{\omega_M} \right) \\ &\times \left[\tilde{\rho}_{2,\bar{n}}(u, \omega, \xi) - \frac{1}{2\omega_M} \tilde{\rho}_{3,\bar{n}}(u, \omega, \xi) \right] \Big|_{u=\frac{\omega' - \omega_c - \omega}{\xi}}, \end{aligned} \quad (69)$$

$$\begin{aligned} \mathcal{F}_{3P,n}(\omega_s, \omega_M) &= \int_0^{\omega_s - \omega_c} d\omega \int_{\omega_s - \omega_c - \omega}^{\infty} \frac{d\xi}{\xi} \text{Exp} \left(-\frac{\omega_s}{\omega_M} \right) \tilde{\rho}_{2,n}(u, \omega, \xi) \Big|_{u=\frac{\omega_s - \omega_c - \omega}{\xi}} \\ &+ \int_{\omega_c}^{\omega_s} d\omega' \int_0^{\omega' - \omega_c} d\omega \int_{\omega' - \omega_c - \omega}^{\infty} \frac{d\xi}{\xi} \frac{1}{\omega_M} \text{Exp} \left(-\frac{\omega'}{\omega_M} \right) \tilde{\rho}_{2,n}(u, \omega, \xi) \Big|_{u=\frac{\omega' - \omega_c - \omega}{\xi}}. \end{aligned} \quad (70)$$

It is evident from (68) that the large-recoil symmetry breaking effect between the vector and scalar $B \rightarrow D$ form factors can be induced by the higher-twist contributions from the three-particle B -meson DA, already at tree level.

We are now ready to derive the power counting behaviour of the three-particle correction to $B \rightarrow D$ form factors at tree level. Applying the canonical behaviour of the three-particle B -meson DA in the end-point region [7]

$$\Psi_V(\omega, \xi) \sim \Psi_A(\omega, \xi) \sim \xi^2, \quad X_A(\omega, \xi) \sim \xi(2\omega - \xi), \quad Y_A(\omega, \xi) \sim \xi, \quad (71)$$

we can verify that the three-particle contribution to the sum rules of $B \rightarrow D$ form factors (68) is counted as $\mathcal{O}((\Lambda/m_b)^{3/2})$ in the heavy quark limit and is indeed suppressed by a factor of Λ/m_b compared to the two-particle contribution at tree level as presented in (9). However, it needs to point out that higher twist effects from the three-particle gluon-quark DA can give rise to the leading power contributions to $B \rightarrow D$ form factors at $\mathcal{O}(\alpha_s)$ on account of the reasonings of [50, 51] and a transparent demonstration of this observation by computing the three-particle contribution to the sum rules at NLO in α_s directly is in high demand on both conceptual and phenomenological aspects.

The final expressions for the form factors of $B \rightarrow D\ell\nu$ can be obtained by adding up the two-particle and the three-particle contributions together

$$f_{BD}^+(q^2) = f_{BD,2P}^+(q^2) + f_{BD,3P}^+(q^2), \quad f_{BD}^0(q^2) = f_{BD,2P}^0(q^2) + f_{BD,3P}^0(q^2), \quad (72)$$

where the detailed expressions of $f_{BD,2P}^{+,0}(q^2)$ and $f_{BD,3P}^{+,0}(q^2)$ are presented in (62) and (68), respectively.

5 Numerical analysis

Having at our disposal the resummation improved sum rules for $B \rightarrow D$ form factors, we are in a position to explore the phenomenological consequences of perturbative corrections to the two-particle contributions and higher-twist effects from the three-particle quark-gluon B -meson DA at tree level. Employing the obtained theory predictions for $B \rightarrow D$ form factors, we will further present our results for the semileptonic $B \rightarrow D\ell\nu$ ($\ell = \mu, \tau$) decay observables, including the invariant-mass distributions of the lepton pair, the topical $R(D)$ ratio, and the CKM matrix element $|V_{cb}|$.

5.1 Theory input parameters

We will first specify the theory inputs entering the LCSR for $B \rightarrow D$ form factors shown in (62) and (68). The fundamental nonperturbative quantities describing the soft strong interaction dynamics encoded in the correlation function (1) are the B -meson light-cone DA defined in (4) and (66). A detailed account of the current understanding towards perturbative and nonperturbative aspects of the two-particle B -meson DA was already presented in [15], following which we will consider two models of the leading twist DA $\phi_B^+(\omega, \mu_0)$ proposed in [34, 52]

$$\phi_{B,\text{I}}^+(\omega, \mu_0) = \frac{\omega}{\omega_0^2} e^{-\omega/\omega_0}, \quad (73)$$

$$\phi_{B,\text{II}}^+(\omega, \mu_0) = \frac{1}{4\pi \omega_0} \frac{k}{k^2 + 1} \left[\frac{1}{k^2 + 1} - \frac{2(\sigma_1(\mu_0) - 1)}{\pi^2} \ln k \right], \quad k = \frac{\omega}{1 \text{ GeV}}, \quad (74)$$

where the shape parameter ω_0 can be converted to the inverse moment of the leading-twist B -meson DA $\lambda_B(\mu_0)$. The renormalization scale evolution of $\lambda_B(\mu)$ at one loop can be derived from the Lange-Neubert equation of $\phi_B^+(\omega, \mu)$ [53]

$$\frac{\lambda_B(\mu_0)}{\lambda_B(\mu)} = 1 + \frac{\alpha_s(\mu_0) C_F}{4\pi} \ln \frac{\mu}{\mu_0} \left[2 - 2 \ln \frac{\mu}{\mu_0} - 4\sigma_1(\mu_0) \right] + \mathcal{O}(\alpha_s^2). \quad (75)$$

The inverse-logarithmic moment at a hadronic scale $\mu_0 = 1 \text{ GeV}$ will be taken as $\sigma_1(\mu_0) = 1.4 \pm 0.4$, determined from a QCD sum rule analysis [52]. The higher-twist two-particle DA of the B -meson $\phi_B^-(\omega, \mu_0)$ will be determined from the QCD equations of motion in the heavy quark limit [45]

$$\omega \phi_B^-(\omega) - \int_0^\omega d\eta [\phi_B^-(\eta) - \phi_B^+(\eta)] = 2 \int_0^\omega d\eta \int_{\omega-\eta}^\infty \frac{d\xi}{\xi} \frac{\partial}{\partial \xi} [\Psi_A(\eta, \xi) - \Psi_V(\eta, \xi)], \quad (76)$$

which was also demonstrated to be valid from a non-relativistic toy model manifestly at NLO in the strong coupling constant [39]. With regarding to the three-particle quark-gluon DA of the B -meson, we will employ the exponential model inspired from the canonical behaviour predicted by the HQET sum rules at tree level [7]

$$\Psi_V(\omega, \xi, \mu_0) = \Psi_A(\omega, \xi, \mu_0) = \frac{\lambda_E^2}{6\omega_0^4} \xi^2 e^{-(\omega+\xi)/\omega_0},$$

$$X_A(\omega, \xi, \mu_0) = \frac{\lambda_E^2}{6\omega_0^4} \xi (2\omega - \xi) e^{-(\omega+\xi)/\omega_0},$$

$$Y_A(\omega, \xi, \mu_0) = -\frac{\lambda_E^2}{24\omega_0^4} \xi (7\omega_0 - 13\omega + 3\xi) e^{-(\omega+\xi)/\omega_0}, \quad (77)$$

where the normalization constant defined by the matrix element of the chromoelectric operator was estimated as $\lambda_E^2(\mu_0) = (0.03 \pm 0.02) \text{ GeV}^2$ [54], from the two-point QCD sum rules including higher-order perturbative and nonperturbative corrections. We already implemented the approximation $\lambda_E = \lambda_H$ in the above expressions, following [7], which is supported by the nonperturbative QCD calculations numerically [34, 54].

With the matching relation (6) the static B -meson decay constant $\tilde{f}_B(\mu)$ can be traded into the QCD decay constant f_B , whose values will be taken from lattice QCD simulations $f_B = (192.0 \pm 4.3) \text{ MeV}$ [55] with $N_f = 2+1$. Likewise, we will adopt the intervals for the D -meson decay constant in QCD from lattice simulations $f_D = (209.2 \pm 3.3) \text{ MeV}$ [55] with $N_f = 2+1$. In addition, we will employ the $\overline{\text{MS}}$ bottom quark mass $\overline{m_b}(\overline{m_b}) = (4.193_{-0.035}^{+0.022}) \text{ GeV}$ [56] from non-relativistic sum rules and the $\overline{\text{MS}}$ charm quark mass $\overline{m_c}(\overline{m_c}) = (1.288 \pm 0.020) \text{ GeV}$ [57] from relativistic sum rules, employing the quark vector correlation function computed at $\mathcal{O}(\alpha_s^3)$. Following [15, 41], the hard scales μ_{h1} and μ_{h2} are taken to be equal and will be varied in the interval $[m_b, 2m_b]$ around the default value m_b , and the factorization scale is chosen as $1.0 \text{ GeV} \leq \mu \leq 2.0 \text{ GeV}$ with the default value $\mu = 1.5 \text{ GeV}$.

The determination of the sum rule parameters ω_M and ω_s can be achieved by implementing the standard procedure described in [15] and applying the same strategies leads to

$$M^2 \equiv n \cdot p \omega_M = (4.5 \pm 1.0) \text{ GeV}^2, \quad s_0 \equiv n \cdot p \omega_s = (6.0 \pm 0.5) \text{ GeV}^2, \quad (78)$$

which respect the power counting rules for the Borel mass and the threshold parameter displayed in (10) and are also in agreement with the intervals adopted in [10, 58].

5.2 Predictions for $B \rightarrow D$ form factors

We will turn to discuss the choice of the inverse moment $\lambda_B(1 \text{ GeV})$ which serves as an important source for theory uncertainties, prior to presenting the sum rule predictions for the form factors of $B \rightarrow D\ell\nu$. Albeit with the intensive investigations of determining λ_B theoretically, the current constraints on λ_B are still far from satisfactory, due to the emerged tension between the NLO sum rule predictions and the implications of hadronic B -meson decay data from QCD factorization. In particular, the subleading power contributions in HQE can give rise to sizeable impact on the determination of λ_B numerically. This has been demonstrated explicitly by extracting λ_B from the partial branching fractions of $B \rightarrow \gamma\ell\nu$ with the power suppressed effects estimated from the dispersion approach [20, 59]. Following the above argument, it is very plausible that the unaccounted subleading power contributions to the LCSR for $B \rightarrow \pi$ form factors can yield significant corrections to the fitted values of $\lambda_B(\mu_0)$ [15] in addition to the systematic uncertainty induced by the parton-hadron duality approximation. In order to be insensitive to the unconsidered effects in the sum rule determinations [15], we will perform an independent determination of $\lambda_B(\mu_0)$ by matching the B -meson LCSR of the

vector $B \rightarrow D$ form factor at $q^2 = 0$ to the lattice-QCD calculation with an extrapolation to the large recoil region using the z -series parametrization. Taking $f_{BD}^+(0) = 0.672 \pm 0.027$ [4] as an input and implementing the above-mentioned matching procedure lead to

$$\begin{aligned}\omega_0(1 \text{ GeV}) &= 570_{-35}^{+38} \text{ MeV}, & (\text{Model I}) \\ \omega_0(1 \text{ GeV}) &= 555_{-20}^{+24} \text{ MeV}, & (\text{Model II})\end{aligned}\quad (79)$$

which differ from the intervals of $\lambda_B(\mu_0)$ obtained from matching two different versions of sum rules for the vector $B \rightarrow \pi$ form factor [15], however, are comparable to the values determined with distinct QCD approaches [52, 60]. In the following we will take $\phi_{B,I}^+(\omega, \mu_0)$ as our default model for the illustration purpose and the systematic uncertainty induced by the model dependence of $\phi_B^+(\omega, \mu_0)$ will be taken into account in the final predictions for the form factors of $B \rightarrow D\ell\nu$.

Now we are ready to explore the numerical features of the LCSR predictions for $B \rightarrow D$ form factors including the NLL resummation for the two-particle contributions and the subleading power corrections from the three-particle quark-gluon DA. To demonstrate the reliability of the sum rule calculations, we first display the dependence of $f_{BD}^+(0)$ on the sum rule parameters M^2 and s_0 in figure 4. It is apparent that the variations of the Borel parameter and the effective threshold within the intervals (78) only bring about negligible influence on the sum rule predictions for the vector form factor of $B \rightarrow D\ell\nu$. We further present the separate contributions to $f_{BD}^+(0)$ from the two-particle and the three-particle contributions in figure 4 in an attempt to understand the subleading power corrections from the higher Fock states. It can be readily observed that the tree-level contributions from the three-particle B -meson DA turn out to be of minor importance numerically, approximately $\mathcal{O}(1\%)$, compared to the two-particle contributions. However, it is worthwhile to mention that the smallness of the three-particle contribution at leading order (LO) in perturbative expansion does not imply the insignificant impact of the subleading power contributions in the $B \rightarrow D\ell\nu$ decay amplitude in general, due to the yet unaccounted power suppressed effects induced by the off light-cone corrections to the nonlocal matrix element defining the two-particle B -meson DA, by the subleading power corrections to the perturbative coefficient functions entering the factorization formula (11) and by the additional contributions generated by new momentum regions (or equivalently, new field modes in the language of SCET) when applying the method of regions to the evaluation of loop integrals involved in perturbative corrections to the QCD amplitude.

We proceed to investigate the impact of perturbative corrections to the short-distance functions and resummation effects for the parametrically large logarithms on predicting the form factors of $B \rightarrow D\ell\nu$. It is evident from figure 5 that NLO QCD corrections to the perturbative matching coefficients can reduce the tree-level prediction for $f_{BD}^+(0)$ by approximately 10% at $\mu = 1.5 \text{ GeV}$ and the NLL resummation effect can enhance the NLO QCD calculation by an amount of 3% numerically at the same value of μ . Both the NLO and NLL predictions exhibit much weaker dependencies on the factorization scale when compared to the LO result. Inspecting the different origins of perturbative QCD corrections displayed in figure 5 shows that the one-loop hard-collinear correction turns out to be more pronounced than the corresponding hard correction, with the inverse moment $\lambda_B(\mu_0) = 570 \text{ MeV}$, at $q^2 \geq 0$, highlighting the

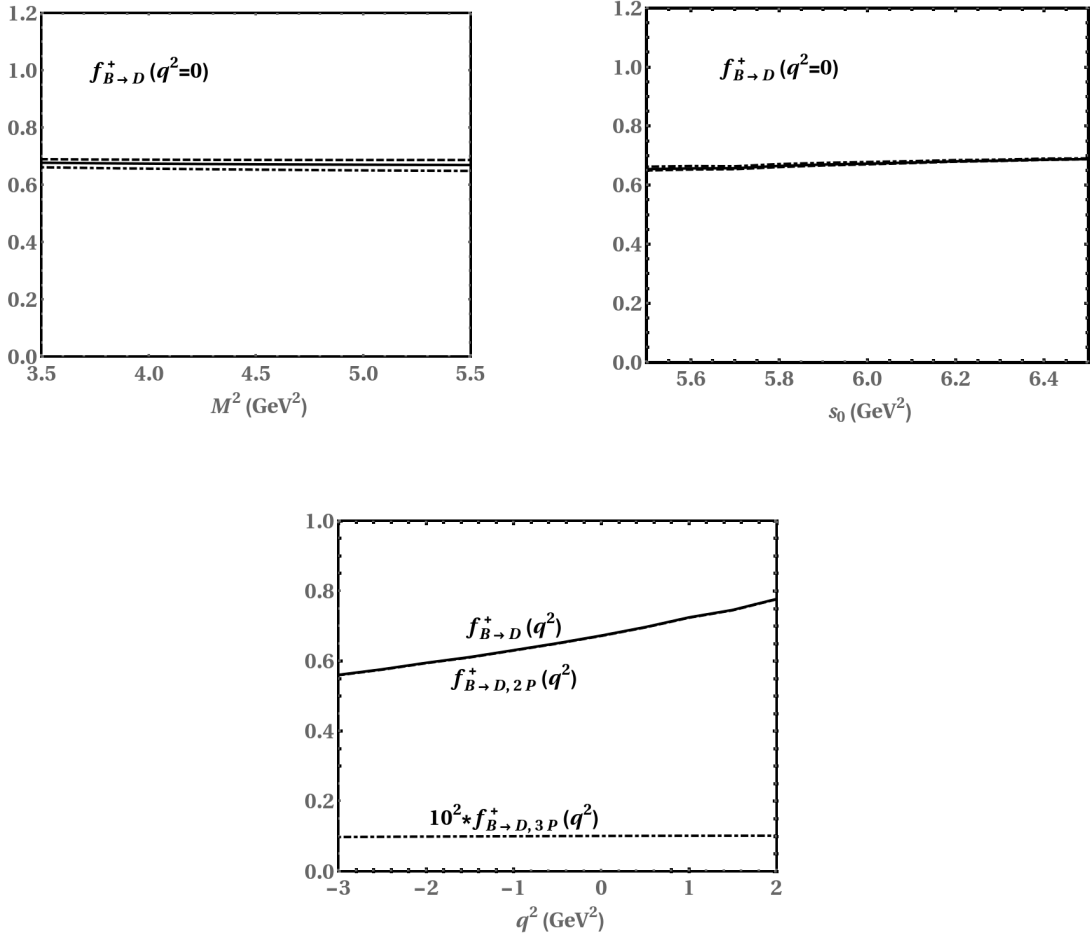


Figure 4: **Top:** Dependence of the vector form factor $f_{BD}^+(0)$ on the Borel mass M^2 (left panel) and on the duality-threshold parameter s_0 (right panel) at $\lambda_B(\mu_0) = 570$ MeV. The solid, dashed and dot-dashed curves are predicted from the LCSR (72) with $s_0 = 6.0$ GeV 2 , 6.5 GeV 2 and 5.5 GeV 2 (left panel), and with $M^2 = 4.5$ GeV 2 , 5.5 GeV 2 and 3.5 GeV 2 (right panel). **Bottom:** Breakdown of the form factor $f_{BD}^+(0)$ from the two-particle and from the three-particle contributions. The two-particle contribution to $f_{BD}^+(0)$ indicated by the dashed curve is almost indistinguishable from the total result represented by the solid curve, due to the negligible effect from the three-particle B -meson DA as shown by the dot-dashed curve.

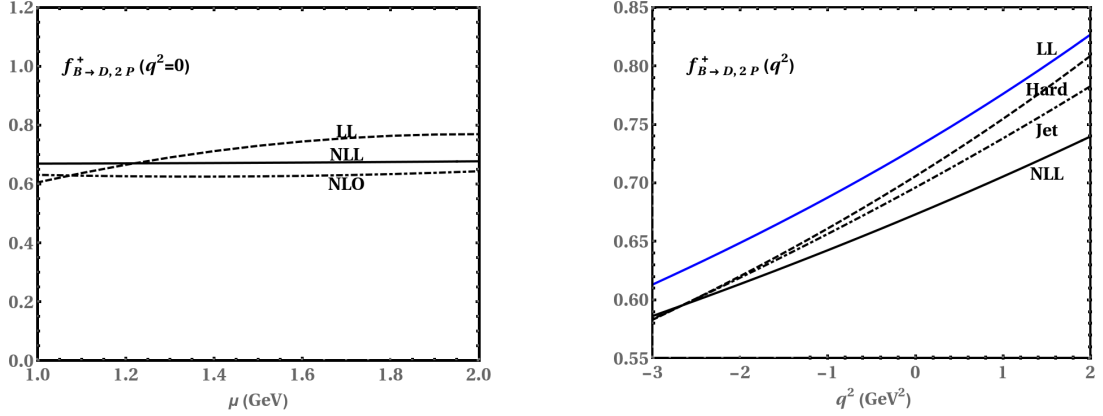


Figure 5: **Left:** Factorization scale dependence of the two-particle contributions to the form factor $f_{BD}^+(0)$ computed from the sum rules (62). The curves labelled with “LL”, “NLO” and “NLL” are obtained from the resulting predictions at leading-logarithmic (LL), NLO and NLL accuracy. **Right:** Breakdown of the two-particle contributions to $f_{BD}^+(0)$ from the LL effect, from the NLL hard correction (“Hard”) and from the NLL hard-collinear correction (“Jet”).

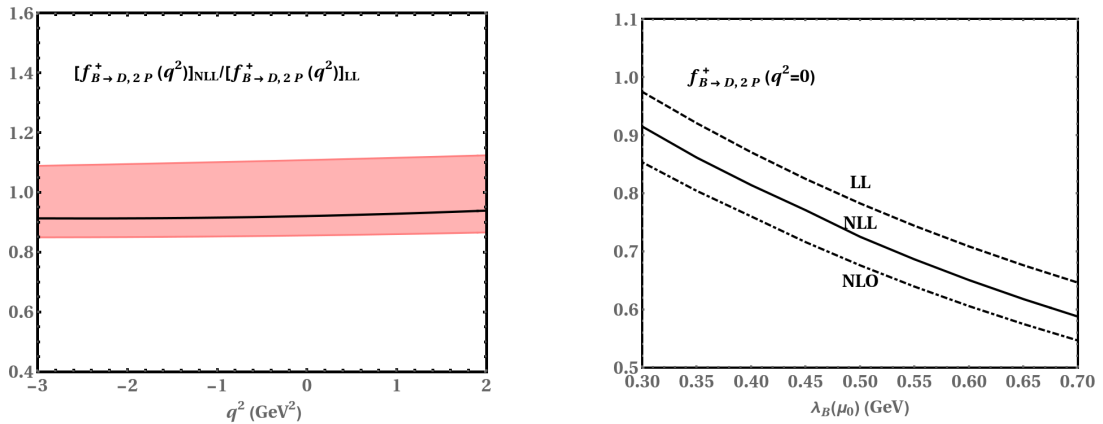


Figure 6: **Left:** The q^2 dependence of the ratio $[f_{BD,2P}^+(q^2)]_{\text{NLL}}/[f_{BD,2P}^+(q^2)]_{\text{LL}}$ with uncertainties from the variations of both the hard and hard-collinear scales. **Right:** Dependence of the two-particle contributions to $f_{BD}^+(q^2 = 0)$, at LL, NLO and NLL accuracy, on the inverse moment of the leading twist B -meson DA $\lambda_B(\mu_0)$.

significance of computing the NLO jet functions accomplished in this paper. We further plot the theory predictions for the ratio $[f_{BD,2P}^+(q^2)]_{\text{NLL}}/[f_{BD,2P}^+(q^2)]_{\text{LL}}$ in figure 6 with uncertainties from the variations of both the hard and hard-collinear scales within the intervals given above. To develop a better understanding of the sensitivity of $B \rightarrow D$ form factors on the inverse moment λ_B , we also present the LO, NLO and NLL sum rule predictions for the leading power contributions to $f_{BD}^+(q^2)$, in figure 6, in a wide range $300 \text{ MeV} \leq \lambda_B(\mu_0) \leq 700 \text{ MeV}$. We can readily observe that the sum rule predictions for $f_{BD}^+(q^2)$ increase steadily with the reduction of λ_B , in analogy to the observation for the radiative leptonic $B \rightarrow \gamma \ell \nu$ decay in [20].

As already explained in [10], the light-cone OPE for the vacuum-to- B -meson correlation function (1) can be only justified near the maximal recoil to fulfill the power counting rules $n \cdot p \gg m_c \gg \Lambda$ and $m_c \sim \mathcal{O}(\sqrt{n \cdot p \Lambda})$. In addition, QCD factorization for the correlation function (1) is fully applicable at space-like momentum transfer on the basis of the power counting analysis. It is then distinctly that the B -meson LCSR for the form factors of $B \rightarrow D \ell \nu$ derived in (72) can be trusted at $q_{min}^2 \leq q^2 \leq q_{max}^2 = 2 \text{ GeV}^2$, where a moderate value $q_{min}^2 = -3 \text{ GeV}^2$ will be employed (see also [58]) in the following analysis for the sake of adopting the same intervals of the sum rules parameters shown in (78). In order to access the information of $B \rightarrow D$ form factors in the whole kinematic region, we need to extrapolate the LCSR predictions obtained above toward large momentum transfer with a certain parametrization for the form factors. Following the arguments of [32, 58], we will take advantage of the z -series parametrization, in line with the analytical properties and perturbative QCD scaling behaviours of $B \rightarrow D$ form factors, which can be readily introduced by mapping the cut complex q^2 -plane onto the unit disk $|z(q^2, t_0)| \leq 1$ according to the conformal transformation [61]

$$z(q^2, t_0) = \frac{\sqrt{t_+ - q^2} - \sqrt{t_+ - t_0}}{\sqrt{t_+ - q^2} + \sqrt{t_+ - t_0}}. \quad (80)$$

Here, the parameter $t_+ = (m_B + m_D)^2$ is determined by the onset of the branching cut in the $|B D\rangle$ channel, and $t_0 < t_+$ is an auxiliary parameter determining the value of q^2 mapped to the origin in the z -plane. An optimal choice of $t_0 = (m_B - m_D)^2$ will be implemented in the numerical computation to achieve a narrow interval of $|z|$.

Taking into account the near-threshold behaviour from angular momentum conservation leads to the suggested parametrization [32, 58]

$$f_{BD}^+(q^2) = \frac{f_{BD}^+(0)}{1 - q^2/m_{B_c^*}^2} \left\{ 1 + \sum_{k=1}^{N-1} b_k \left(z(q^2, t_0)^k - z(0, t_0)^k - (-1)^{N-k} \frac{k}{N} [z(q^2, t_0)^N - z(0, t_0)^N] \right) \right\} \quad (81)$$

for the vector form factor, where $m_{B_c^*} = (6.330 \pm 0.009) \text{ GeV}$ [62], and the z -series expansion will be truncated at $N = 2$ in the practical matching procedure. Along the same vein, we will employ the following parametrization

$$f_{BD}^0(q^2) = \frac{f_{BD}^0(0)}{1 - q^2/m_{B_c^{(0)}}^2} \left\{ 1 + \sum_{k=1}^N \tilde{b}_k \left(z(q^2, t_0)^k - z(0, t_0)^k \right) \right\} \quad (82)$$

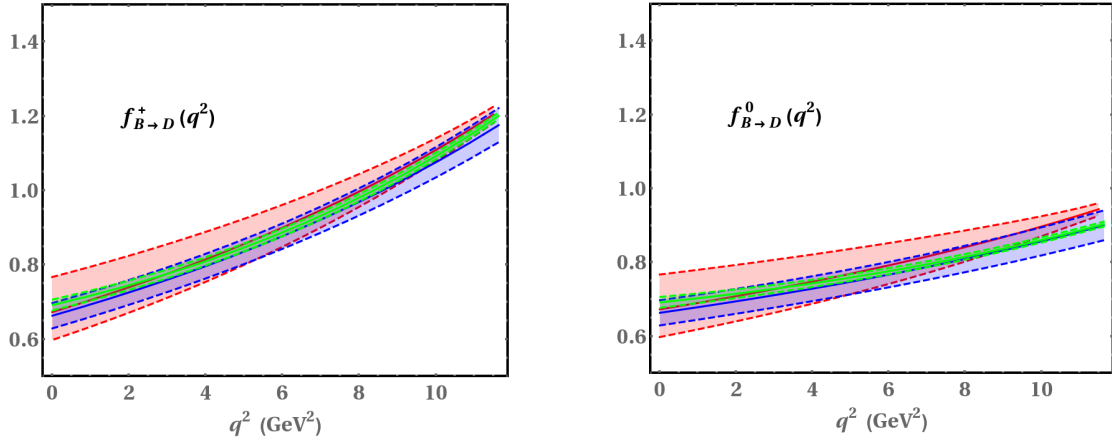


Figure 7: The transfer momentum dependence of the form factor $f_{BD}^+(q^2)$ (left panel) and of the form factor $f_{BD}^0(q^2)$ (right panel) predicted from the LCSR calculations, including the two-particle contributions at NLL accuracy and the tree-level three-particle contributions, with extrapolation toward large q^2 applying the z -series parametrization. The pink, blue and green curves correspond to theory predictions from this work, from the lattice QCD calculations by the HPQCD Collaboration [5], and from a combined fit of the BarBar and Belle data as well as the HPQCD and FNAL/MILC calculations [65]. Theory uncertainties for all the calculations are indicated by the shaded regions.

for the scalar form factor, where $m_{B_c^{(0)}} = (6.420 \pm 0.009)$ GeV [5], and we will only keep the terms up to $\mathcal{O}(z)$ in the z -expansion. An alternative parametrization of $B \rightarrow D$ form factors proposed in [63] (see also [64] for a recent discussion) including the outer function and the Blaschke factor will not be considered here following the reasonings of [32].

Parameter	Central value	ω_0	σ_1	μ	$\mu_{h1(2)}$	M^2	s_0	$\phi_B^\pm(\omega)$
$f_{BD}^+(0)$	0.673	-0.027 +0.026	-0.01 +0.01	+0.015 -0.031	+0.058 -0.035	-0.003 +0.005	+0.015 -0.019	-
b_1	-4.20	-0.80 +0.74	-0.31 +0.30	+0.19 -0.14	+1.51 -1.02	-0.06 +0.14	+0.44 -0.56	+0.11 -0.00
\tilde{b}_1	-0.18	-0.66 +0.60	-0.26 +0.25	+0.17 -0.14	+1.23 -0.84	-0.05 +0.10	+0.36 -0.46	+0.10 -0.00

Table 1: Summary of the predicted shape parameters and the normalization constant entering the z -series parametrizations (81) and (82) for the $B \rightarrow D\ell\nu$ form factors with dominant uncertainties from the variations of theory inputs.

It is now a straightforward task to implement the matching procedure described above

with the aid of the LCSR predictions at $q_{min}^2 \leq q^2 \leq q_{max}^2$ and the z -series parametrization for the determination of the momentum-transfer dependence in the entire kinematic region. To achieve a better accuracy for the resulting shape parameters b_1 and \tilde{b}_1 , we will further employ the synthetic data points for the form factors $f_{BD}^{+,0}(q^2)$ at $q^2 = 8.47 \text{ GeV}^2$, 10.05 GeV^2 and 11.63 GeV^2 from the FNAL/MILC Collaboration [4] in the numerical fitting. We present the yielding predictions for the q^2 dependence of $f_{BD}^{+,0}(q^2)$ in the physical kinematic range $0 \leq q^2 \leq (m_B - m_D)^2$ with theory uncertainties in figure 7 where recent determinations from the lattice QCD simulation combined with a similar z -parametrization by the HPQCD Collaboration [5] and from a joint fit of the BaBar and Belle data combined with the lattice calculations [65] are also shown for a comparison. It is apparent that our predictions for the $B \rightarrow D\ell\nu$ form factors are in good agreement with those displayed in [5, 65] within the theory uncertainties. We further collect the obtained results for the shape parameters, with numerically important uncertainties, entering the z -series expansion in Table 1, where the predictions for form factors at $q^2 = 0$ are also presented for completeness. It turns out that the dominant theory uncertainties for the shape parameters arise from the variations of the hard scales $\mu_{h1(2)}$ and from the errors in the determination of ω_0 . The relatively more precise predictions for the form factors of $B \rightarrow D\ell\nu$ at high q^2 are mainly due to the high precision lattice date points from the FNAL/MILC Collaboration [4], whose accuracy is even significantly better than that computed by the HPQCD Collaboration [5]. Moreover, the LCSR predictions for $f_{BD}^{+,0}(q^2)$ appear to grow faster with the increase of the momentum transfer squared compared to those obtained from the lattice calculations [5].

Another popular parametrization for the form factors of $B \rightarrow D\ell\nu$ taking into account the constraints from the heavy quark symmetry, proposed in [33], was also extensively employed in the phenomenological applications. Including the subleading power corrections to the heavy-quark relations and implementing the dispersive analysis yield the following one-parameter representations for the vector and scalar form factors [33, 64]

$$f_{BD}^+(z) = f_{BD}^+(0) [1 - 8\rho^2 z + (51\rho^2 - 10)z^2 - (252\rho^2 - 84)z^3], \quad (83)$$

$$\frac{f_{BD}^0(z)}{f_{BD}^+(z)} = \left(\frac{2\sqrt{r}}{1+r}\right)^2 \frac{1+\omega}{2} 1.0036 [1 + 0.0068\bar{\omega} + 0.0017\bar{\omega}^2 + 0.0013\bar{\omega}^3], \quad (84)$$

where we have introduced the following conventions

$$z = \frac{\sqrt{1+\omega} - \sqrt{2}}{\sqrt{1+\omega} + \sqrt{2}}, \quad \omega = \frac{m_B^2 + m_D^2 - q^2}{2m_B m_D}, \quad \bar{\omega} = 1 - \omega, \quad r = m_D/m_B. \quad (85)$$

Apparently, this z parameter is equivalent to $z(q^2, t_0)$, defined by (80), with $t_0 = (m_B - m_D)^2$. It needs to point out that the ratio $f_{BD}^0(z)/f_{BD}^+(z)$ is fully determined in HQET including both perturbative corrections to the leading Wilson coefficients and subleading power contributions computed from QCD sum rules. Matching the LCSR calculations for the form factors of $B \rightarrow D\ell\nu$ at $q_{min}^2 \leq q^2 \leq q_{max}^2$ onto the CLN parametrization (84) leads to

$$f_{BD}^+(z=0) = 1.22 \pm 0.02, \quad \rho = 1.07^{+0.08}_{-0.11}, \quad (86)$$

which are well consistent with the fitted values obtained in [5], albeit with the comparably large theory uncertainties for the slop parameter ρ .

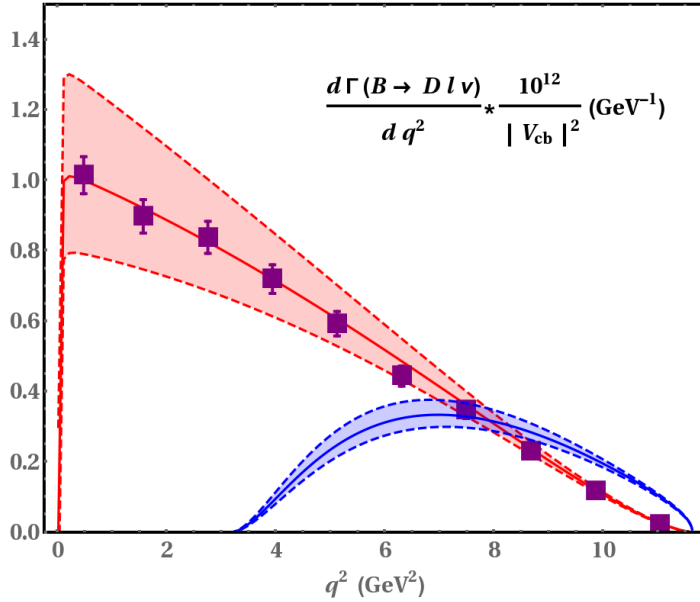


Figure 8: The differential decay rates for $B \rightarrow D\mu\nu_\mu$ (pink band) and $B \rightarrow D\tau\nu_\tau$ (blue band) as a function of the momentum transfer squared q^2 , where the experimental data points for $B \rightarrow D\mu\nu_\mu$ (purple squares) from the Belle Collaboration [68] are also presented for a comparison.

5.3 Phenomenological implications

Having in our hands the theory predictions of the two form factors $f_{BD}^{+,0}(q^2)$, we are ready to explore their phenomenological implications on the semileptonic $B \rightarrow D\ell\nu$ decays. The differential decay rate of $B \rightarrow D\ell\nu$ in the rest frame of the B -meson can be computed as

$$\begin{aligned} \frac{d\Gamma(B \rightarrow D\ell\nu)}{dq^2} &= \frac{\eta_{\text{EW}}^2 G_F^2 |V_{cb}|^2}{24\pi^3 m_B^2} \left(1 - \frac{m_l^2}{q^2}\right)^2 |\vec{p}_D| \left[\left(1 + \frac{m_l^2}{2q^2}\right) m_B^2 |\vec{p}_D|^2 |f_{BD}^+(q^2)|^2 \right. \\ &\quad \left. + \frac{3m_l^2}{8q^2} (m_B^2 - m_D^2)^2 |f_{BD}^0(q^2)|^2 \right], \end{aligned} \quad (87)$$

where $|\vec{p}_D| = \sqrt{\lambda(m_B^2, m_D^2, q^2)/(2m_B)}$ with $\lambda(a, b, c) = a^2 + b^2 + c^2 - 2ab - 2ac - 2bc$ is the magnitude of the three-momentum of the D -meson and

$$\eta_{\text{EW}} = 1 + \frac{\alpha_{\text{em}}}{\pi} \ln \left(\frac{m_Z}{m_B} \right) \simeq 1.0066 \quad (88)$$

originates from the short-distance QED corrections to the four-fermion operator responsible for the $B \rightarrow D\ell\nu$ decays [66, 67]. The differential q^2 distributions for $B \rightarrow D\ell\nu$ obtained

with the form factors $f_{BD}^{+,0}(q^2)$ displayed in Table 1 are plotted in figure 8, including also the recent experimental measurements for the combination of $B^+ \rightarrow \bar{D}^0 e^+ \nu_e$, $B^0 \rightarrow D^- e^+ \nu_e$, $B^+ \rightarrow \bar{D}^0 \mu^+ \nu_\mu$ and $B^0 \rightarrow D^- \mu^+ \nu_\mu$ from the Belle Collaboration [68]. It is evident that our predictions for the q^2 shape of $B \rightarrow D\mu\nu_\mu$ are in excellent agreement with the experimental data bins. Furthermore, we collect the numerical results for the (normalized) partial decay rates of $B \rightarrow D\ell\nu$

$$\Delta\Gamma_\ell(t_1, t_2) = \int_{t_1}^{t_2} dq^2 \frac{d\Gamma(B \rightarrow D\ell\nu)}{dq^2} \frac{1}{|V_{cb}|^2} \quad (89)$$

in Tables 2 and 3 with selections of the q^2 bins identical to that from the Belle and BaBar measurements [68, 69].

$[t_1, t_2]$ (GeV 2)	$\Delta\Gamma_\mu(t_1, t_2)$ this work	(10^{-12} GeV) Belle [68]	$[t_1, t_2]$ (GeV 2)	$\Delta\Gamma_\mu(t_1, t_2)$ this work	(10^{-12} GeV) Belle [68]
[0.00, 0.98]	$1.00_{-0.21}^{+0.28}$	1.01 ± 0.05	[5.71, 6.90]	$0.57_{-0.06}^{+0.08}$	0.53 ± 0.03
[0.98, 2.16]	$1.09_{-0.21}^{+0.27}$	1.06 ± 0.06	[6.90, 8.08]	$0.43_{-0.04}^{+0.05}$	0.41 ± 0.03
[2.16, 3.34]	$0.97_{-0.16}^{+0.21}$	0.99 ± 0.05	[8.08, 9.26]	$0.28_{-0.02}^{+0.02}$	0.27 ± 0.02
[3.34, 4.53]	$0.85_{-0.13}^{+0.16}$	0.85 ± 0.05	[9.26, 10.45]	$0.14_{-0.01}^{+0.01}$	0.14 ± 0.01
[4.53, 5.71]	$0.72_{-0.09}^{+0.11}$	0.70 ± 0.04	[10.45, 11.63]	$0.03_{-0.00}^{+0.00}$	0.02 ± 0.01

Table 2: Theory predictions for the partial decay rates of $B \rightarrow D\mu\nu_\mu$ compared with the Belle measurements from [68].

In particular, our predictions for the total decay width of $B \rightarrow D\mu\nu_\mu$ in units of $1/|V_{cb}|^2$ can be obtained straightforwardly

$$\Delta\Gamma_\mu(0, 11.63 \text{ GeV}^2) = (6.06_{-0.92}^{+1.18}) \times 10^{-12} \text{ GeV}, \quad (90)$$

with all separate uncertainties from variations of the theory inputs added in quadrature, from

$[t_1, t_2]$ (GeV 2)	$\Delta\Gamma_\tau(t_1, t_2)$ (10 $^{-12}$ GeV) this work	$\Delta\mathcal{R}(t_1, t_2)$	
		this work	[71]
[4.00, 4.53]	$0.073^{+0.014}_{-0.011}$	$0.199^{+0.002}_{-0.002}$	0.199 ± 0.001
[4.53, 5.07]	$0.11^{+0.02}_{-0.02}$	$0.331^{+0.003}_{-0.003}$	0.330 ± 0.001
[5.07, 5.60]	$0.14^{+0.02}_{-0.02}$	$0.458^{+0.004}_{-0.004}$	0.455 ± 0.001
[5.60, 6.13]	$0.16^{+0.02}_{-0.02}$	$0.575^{+0.006}_{-0.005}$	0.571 ± 0.002
[6.13, 6.67]	$0.18^{+0.02}_{-0.02}$	$0.687^{+0.007}_{-0.006}$	0.680 ± 0.002
[6.67, 7.20]	$0.18^{+0.02}_{-0.02}$	$0.796^{+0.008}_{-0.007}$	0.786 ± 0.003
[7.20, 7.73]	$0.17^{+0.02}_{-0.02}$	$0.905^{+0.009}_{-0.007}$	0.892 ± 0.003
[7.73, 8.27]	$0.17^{+0.02}_{-0.01}$	$1.024^{+0.009}_{-0.008}$	1.006 ± 0.004
[8.27, 8.80]	$0.15^{+0.01}_{-0.01}$	$1.161^{+0.010}_{-0.009}$	1.135 ± 0.005
[8.80, 9.33]	$0.14^{+0.01}_{-0.01}$	$1.329^{+0.011}_{-0.009}$	1.294 ± 0.006
[9.33, 9.86]	$0.12^{+0.01}_{-0.01}$	$1.561^{+0.011}_{-0.010}$	1.513 ± 0.007
[9.86, 10.40]	$0.099^{+0.006}_{-0.005}$	$1.934^{+0.012}_{-0.010}$	1.86 ± 0.01
[10.40, 11.63]	$0.12^{+0.01}_{-0.01}$	$3.364^{+0.008}_{-0.008}$	—

Table 3: Theory predictions for the partial decay rates of $B \rightarrow D\tau\nu_\tau$ and for the binned distributions of $\Delta\mathcal{R}(t_1, t_2)$ defined in (92). The semileptonic $B \rightarrow D$ form factors obtained by fitting the experimental data with the Boyd-Grinstein-Lebed parametrization [63] are employed for the recent calculations presented in [71].

which the exclusive determinations of $|V_{cb}|$ are achieved

$$|V_{cb}| = \begin{cases} \left(39.2^{+3.4}_{-3.3}\Big|_{\text{th}} \pm 1.0\Big|_{\text{exp}}\right) \times 10^{-3}, & [\text{BaBar 2010}] \\ \left(40.6^{+3.5}_{-3.5}\Big|_{\text{th}} \pm 1.0\Big|_{\text{exp}}\right) \times 10^{-3}, & [\text{Belle 2016}] \end{cases} \quad (91)$$

with the recent experimental measurements of the total branching fraction from the Belle [68] and BaBar [70] Collaborations ¹. The resulting determinations of $|V_{cb}|$ suffer from a sizeable uncertainty, approximately $\mathcal{O}(10\%)$, due to the LCSR calculations of $B \rightarrow D$ form factors at large hadronic recoil. Our results are consistent with the more precise determinations from FNAL/MILC [4], HPQCD [5] and from a joint fit [64] of the available experimental data and the lattice calculations including the updated unitarity bounds.

Finally, we turn to compute the differential distributions of the celebrated ratio

$$\Delta\mathcal{R}(t_1, t_2) = \frac{\int_{t_1}^{t_2} dq^2 d\Gamma(B \rightarrow D\tau\nu_\tau)/dq^2}{\int_{t_1}^{t_2} dq^2 d\Gamma(B \rightarrow D\mu\nu_\mu)/dq^2}, \quad (92)$$

where most of the hadronic uncertainties from the $B \rightarrow D\ell\nu$ form factors are cancelled out. Inspecting the obtained results in Table 3 indeed implies an incredibly precise one-percent accuracy of $\Delta\mathcal{R}(t_1, t_2)$, albeit with the implementation of much less accurate predictions for the hadronic form factors shown in Table 1. Our predictions for the binned distributions of $\Delta\mathcal{R}(t_1, t_2)$ are also compatible with the recent determinations reported in [71], employing the $B \rightarrow D\ell\nu$ form factors extracted from a joint fit of the experimental data and two recent lattice calculations [64]. We further present our predictions for the ratio of the total branching fractions of two semileptonic decay channels

$$R(D) \equiv \frac{\mathcal{BR}(B \rightarrow D\tau\nu_\tau)}{\mathcal{BR}(B \rightarrow D\mu\nu_\mu)} = 0.305^{+0.022}_{-0.025}, \quad (93)$$

which coincides with the previous determinations [4, 5, 64, 71–74] in the Standard Model (SM) at the 1σ level and needs to be compared with the HFAG average value $R(D)|_{\text{HFAG}} = 0.403 \pm 0.040 \pm 0.024$ [2]. We mention in passing that the relatively high theory uncertainty of $R(D)$ in (93), approximately 8%, can be traced back to the uncancelled hadronic uncertainties for determining the partial branching fraction of $B \rightarrow D\mu\nu_\mu$ in the phase-space region $0 \leq q^2 \leq m_\tau^2$.

6 Concluding discussion

In this paper we have presented perturbative QCD corrections to the semileptonic $B \rightarrow D\ell\nu$ form factors with the power counting scheme $m_c \sim \mathcal{O}(\sqrt{\Lambda m_b})$, at leading power in Λ/m_b ,

¹The previous measurements from ALEPH, CLEO, Belle and BaBar summarized by the Heavy Flavor Averaging Group (HFAG) [2] are not considered here. We leave a dedicated study of the $|V_{cb}|$ determination including all the available experimental data and the correlation of theory predictions for the $B \rightarrow D\ell\nu$ form factors at different q^2 for future work.

employing the LCSR with the two-particle B -meson DA. QCD factorization for the vacuum-to- B -meson correlation function (1) was demonstrated explicitly at one loop applying the diagrammatic factorization approach. Apparently, the hard coefficients entering the factorization formulae of (1) can be extracted directly from the perturbative matching coefficients appeared in the SCET representation of the QCD weak current $\bar{q} \gamma_\mu (1 - \gamma_5) b$. Due to the appearance of a new hard-collinear scale m_c , the resulting jet functions determined from the method of regions turn out to be more complex than the counterparts in the evaluation of the correlation function for constructing the sum rules of $B \rightarrow \pi$ form factors. Taking advantage of the evolution equation of the B -meson DA $\phi_B^-(\omega, \mu)$, factorization-scale independence of the correlation function (1) was further verified at $\mathcal{O}(\alpha_s)$ with the obtained hard and hard-collinear functions. QCD resummation for the parametrically large logarithms involved in the short-distance functions at NLL was achieved by employing the corresponding RG equations in momentum space (see [36, 75] for an alternative implementation in “dual” space). The NLL resummation improved sum rules for $B \rightarrow D$ form factors (62) derived with the dispersion representations in Appendix B constitute the main new ingredients of this paper. The subleading power contributions from the three-particle quark-gluon B -meson DA were also computed from the same LCSR method at tree level. In the light of the canonical behaviours of the three-particle DA of the B -meson from the QCD sum rule analysis at tree level [7], the power suppressed three-particle corrections were demonstrated to invalidate the large-recoil symmetry relation between the vector and scalar $B \rightarrow D$ form factors.

We proceeded to explore the phenomenological implications of the resulting sum rules for the $B \rightarrow D\ell\nu$ form factors applying two nonperturbative models for the B -meson DA $\phi_B^+(\omega, \mu_0)$ inspired from the QCD sum rule calculations [34, 52]. The perturbative QCD corrections from the two-particle DA at NLL were found to generate an approximately $\mathcal{O}(10\%)$ shift to the LL predictions for $f_{BD}^+(q^2)$ with the default theory inputs, and the one-loop hard-collinear corrections appear to have a more profound influence at $q^2 \geq 0$ numerically when compared with the corresponding hard corrections. Moreover, the subleading power effects from the three-particle B -meson DA were shown to be insignificant numerically. The z -series expansion fulfilling the analytical properties of $B \rightarrow D$ form factors was further employed to extrapolate the NLL LCSR predictions toward the low recoil region. In addition, we presented theory predictions for the binned distributions of the $B \rightarrow D\ell\nu$ decay rates and of the ratio $\Delta\mathcal{R}(t_1, t_2)$ by applying our determinations of the form factors $f_{BD}^{+,0}(q^2)$. Matching the predicted results for the normalized decay width of $B \rightarrow D\mu\nu_\mu$ and the recent experimental measurements from Belle [68] and BaBar [70] led to the extracted values of $|V_{cb}|$ at $\mathcal{O}(10\%)$ accuracy as displayed in (91). Our predictions for the $B \rightarrow D$ form factors also gave rise to the determinations $R(D) = 0.305^{+0.022}_{-0.025}$, confronted with the HFAG average value $R(D)|_{\text{HFAG}} = 0.403 \pm 0.040 \pm 0.024$ [2]. Improving the theory precision for determining the $B \rightarrow D\ell\nu$ form factors in the large recoil region $0 \leq q^2 \leq m_\tau^2$ will be essential to reduce the theory errors of $R(D)$ in the future.

Further developments of the B -meson LCSR approach for computing the form factors of $B \rightarrow D\ell\nu$ can be pushed forward in distinct directions. First, perturbative QCD corrections to the LCSR (68) from the three-particle B -meson DA can be carried out for a complete understanding of the leading power contributions in the heavy quark limit. In doing so, the one-loop evolution equations for the remaining high-twist three-particle DA of the B -meson in (66) are in demand. Second, computing yet higher-order QCD corrections to the two-particle

contributions (62) are of both conceptual and phenomenological interest for exploring the renormalization properties of the B -meson DA $\phi_B^\pm(\omega, \mu)$ at two loops (e.g., the eigenfunctions and the analytical structures of renormalization kernels) and for bringing down the still sizeable perturbative uncertainties of the theory predictions displayed in Table 1. Third, the present strategies can be readily applied to calculate QCD corrections to the semileptonic $B \rightarrow D^* \ell \nu$ form factors based upon the LCSR with the B -meson DA (with additional attention to the renormalization prescription of γ_5 in dimensional regularization), allowing for a comprehensive analysis of the full angular distributions $B \rightarrow D^*(\rightarrow D X) \tau(\rightarrow Y \nu_\tau) \bar{\nu}_\tau$ with $X = (\pi, \gamma)$ and $Y = (\ell \nu, \pi)$ as discussed in [76]. To conclude, precision QCD calculations of semileptonic B -meson form factors with analytical QCD approaches will continually provide us with a deeper insight into the strong interaction dynamics of heavy quark decays and into the general properties of effective field theories.

Acknowledgements

We are grateful to Carleton DeTar and Heechang Na for providing us with the Lattice QCD results presented in [5, 65]. C.D.L is supported in part by the National Natural Science Foundation of China (NSFC) with Grant Nos. 11375208, 11521505, 11621131001 and 11235005, and by the Open Project Program of State Key Laboratory of Theoretical Physics, Institute of Theoretical Physics, Chinese Academy of Sciences with Grant No. Y5KF111CJ. The work of Y.L.S is supported by Natural Science Foundation of Shandong Province, China under Grant No. ZR2015AQ006. Y.M.W acknowledges support from the National Youth Thousand Talents Program, the Youth Hundred Academic Leaders Program of Nankai University, and the NSFC with Grant No. 11675082. This research was also supported in part by the Munich Institute for Astro- and Particle Physics (MIAPP) of the DFG cluster of excellence “Origin and Structure of the Universe”.

A Loop integrals

Here we collect some useful results for the loop integrals used in the calculations of the vacuum-to- B -meson correlation function (1) at $\mathcal{O}(\alpha_s)$.

$$\begin{aligned}
I_1^{hc} &= \int [dl] \frac{n \cdot (p + l)}{[n \cdot (p + l) \bar{n} \cdot (p - k + l) + l_\perp^2 - m_c^2 + i0][n \cdot l + i0][l^2 + i0]} \\
&= \frac{1}{2} \left\{ \frac{2}{\epsilon^2} + \frac{2}{\epsilon} \left[\ln \frac{\mu^2}{n \cdot p (\omega - \bar{n} \cdot p)} - \ln(1 + r_1) + 1 \right] + \ln^2 \frac{\mu^2}{n \cdot p (\omega - \bar{n} \cdot p)} \right. \\
&\quad + 2 \ln \frac{\mu^2}{n \cdot p (\omega - \bar{n} \cdot p)} - 2 \ln(1 + r_1) \left[\ln \frac{\mu^2}{n \cdot p (\omega - \bar{n} \cdot p)} + 1 \right] + \ln^2(1 + r_1) \\
&\quad \left. + 2 r_1 \ln \left(\frac{r_1}{1 + r_1} \right) - 2 \text{Li}_2 \left(\frac{1}{1 + r_1} \right) + \frac{\pi^2}{6} + 4 \right\}, \tag{94}
\end{aligned}$$

$$I_{2,\alpha\beta} = \int [dl] \frac{l_\alpha (p-l)_\beta}{[l^2 + i0][(p-l)^2 - m_c^2 + i0][(l-k)^2 + i0]} \\ \equiv -\frac{g_{\alpha\beta}}{2} I_{2,a} - \frac{1}{p^2} [k_\alpha k_\beta I_{2,b} - p_\alpha p_\beta I_{2,c} - k_\alpha p_\beta I_{2,d} + p_\alpha k_\beta I_{2,e}] , \quad (95)$$

$$I_{2,a} = \frac{1}{2} \left[\frac{1}{\epsilon} + \ln \left(-\frac{\mu^2}{p^2} \right) - \frac{(1+r_2+r_3)^2}{r_3(1+r_3)} \ln(1+r_2+r_3) + \frac{(1+r_2)^2}{r_3} \ln(1+r_2) \right. \\ \left. - \frac{r_2^2}{1+r_3} \ln r_2 + 3 \right] , \quad (96)$$

$$I_{2,b} = \frac{1}{2r_3^3} \left[(2+2r_2-r_3)r_3 - 2(1+r_2)^2 \ln \left(\frac{1+r_2+r_3}{1+r_2} \right) \right] \\ \times \left[\frac{1}{\epsilon} + \ln \left(-\frac{\mu^2}{p^2} \right) - \ln(1+r_2+r_3) + 3 \right] \\ - \frac{(1+r_2)^2}{r_3^3} \left[\text{Li}_2 \left(\frac{1+r_3}{1+r_2+r_3} \right) - \text{Li}_2 \left(\frac{1}{1+r_2} \right) \right] - \frac{(1+r_2)^2}{2r_3^3} \ln^2 \left(\frac{1+r_2+r_3}{1+r_2} \right) \\ + \frac{r_2 [3r_2r_3 + 2(1+r_2+r_3)]}{2r_3^2(1+r_3)^2} \ln \left(\frac{1+r_2+r_3}{r_2} \right) - \frac{1-r_2+r_3}{2r_3(1+r_3)} \quad (97)$$

$$I_{2,c} = \frac{(1+r_3)^2 - r_2^2}{2r_3(1+r_3)^2} \ln \left(\frac{1+r_2+r_3}{1+r_2} \right) + \frac{r_2^2(2+r_3)}{2(1+r_3)^2} \ln \left(\frac{1+r_2}{r_2} \right) - \frac{r_2}{2(1+r_3)} , \quad (98)$$

$$I_{2,d} = \frac{1}{r_3^2} \left[(1+r_2) \ln \left(\frac{1+r_2+r_3}{1+r_2} \right) - r_3 \right] \left[\frac{1}{\epsilon} + \ln \left(-\frac{\mu^2}{p^2} \right) - \ln(1+r_2+r_3) + \frac{5}{2} \right] \\ + \frac{1+r_2}{r_3^2} \left[\text{Li}_2 \left(\frac{1+r_3}{1+r_2+r_3} \right) - \text{Li}_2 \left(\frac{1}{1+r_2} \right) \right] + \frac{1+r_2}{2r_3^2} \ln^2 \left(\frac{1+r_2+r_3}{1+r_2} \right) \\ + \frac{r_2(1-r_3^2+r_2+2r_2r_3)}{2r_3^2(1+r_3)^2} \ln \left(\frac{1+r_2+r_3}{1+r_2} \right) - \frac{r_2[2+r_3(2+r_2)]}{2r_3(1+r_3)^2} \ln \left(\frac{1+r_2}{r_2} \right) \\ - \frac{r_2}{2r_3(1+r_3)} , \quad (99)$$

$$I_{2,e} = -\frac{(1+r_2+r_3)(1+r_2+r_3+2r_2r_3)}{2r_3^2(1+r_3)^2} \ln \left(\frac{1+r_2+r_3}{1+r_2} \right) + \frac{1+r_2+r_3}{2r_3(1+r_3)} \\ + \frac{r_2^2}{2(1+r_3)^2} \ln \left(\frac{1+r_2}{r_2} \right) , \quad (100)$$

$$I_3 = \int [dl] \frac{(n \cdot l)^2}{[l^2 + i0][(p-l)^2 - m_c^2 + i0][(l-k)^2 + i0]} \\ = \frac{(n \cdot p)^2}{2p^2} \left\{ \frac{(1+r_2+r_3)^2}{r_3(1+r_3)^2} \ln \left(\frac{1+r_2+r_3}{1+r_2} \right) - \frac{r_2[2(1+r_3)+r_2(2+r_3)]}{(1+r_3)^2} \ln \left(\frac{1+r_2}{r_2} \right) \right\}$$

$$+ \frac{r_2}{1+r_3} \Big\} , \quad (101)$$

$$I_{4,\alpha} = \int [dl] \frac{l_\alpha}{[l^2 + i0][(p-l)^2 - m_c^2 + i0][(l-k)^2 + i0]} = \frac{1}{p^2} [k_\alpha I_{4,a} + p_\alpha I_{4,b}] , \quad (102)$$

$$\begin{aligned} I_{4,a} &= \left[\frac{1+r_2}{r_3^2} \ln \left(\frac{1+r_2+r_3}{1+r_2} \right) - \frac{1}{r_3} \right] \left[\frac{1}{\epsilon} + \ln \left(-\frac{\mu^2}{p^2} \right) - \ln [(1+r_2)(1+r_2+r_3)] + 2 \right] \\ &\quad + \frac{1+r_2}{r_3^2} \left[\text{Li}_2 \left(\frac{1+r_3}{1+r_2+r_3} \right) - \text{Li}_2 \left(\frac{1}{1+r_2} \right) \right] - \frac{1}{r_3} \ln (1+r_2) \\ &\quad + \frac{1+r_2}{2r_3^2} [\ln^2 (1+r_2+r_3) - \ln^2 (1+r_2)] + \frac{r_2}{r_3(1+r_3)} \ln \left(\frac{r_2}{1+r_2+r_3} \right) , \end{aligned} \quad (103)$$

$$I_{4,b} = \frac{1+r_2+r_3}{r_3(1+r_3)} \ln (1+r_2+r_3) - \frac{1+r_2}{r_3} \ln (1+r_2) + \frac{r_2}{1+r_3} \ln r_2 , \quad (104)$$

$$I_5 = \int [dl] \frac{(2-D)(\not{p}-\not{k}+\not{l}) + D m_c}{[(p-k+l)^2 - m_c^2 + i0][l^2 + i0]} = I_{5,a} (\not{p}-\not{k}) + I_{5,b} m_c , \quad (105)$$

$$I_{5,a} = - \left\{ \frac{1}{\epsilon} + \ln \left(-\frac{\mu^2}{(p-k)^2} \right) + r_1^2 \ln \left(\frac{1+r_1}{r_1} \right) - \ln (1+r_1) + 1 - r_1 \right\} , \quad (106)$$

$$I_{5,b} = 4 \left\{ \frac{1}{\epsilon} + \ln \left(-\frac{\mu^2}{(p-k)^2} \right) - r_1 \ln \left(\frac{1+r_1}{r_1} \right) - \ln (1+r_1) + \frac{3}{2} \right\} , \quad (107)$$

$$\begin{aligned} I_{6,a} &= \int [dl] \frac{n \cdot (p+l)}{[n \cdot (p+l) \bar{n} \cdot (p-k+l) + l_\perp^2 - m_c^2 + i0][n \cdot l \bar{n}(l-k) + l_\perp^2 + i0][l^2 + i0]} \\ &= -\frac{1}{\omega} \left\{ \ln \left(1 - \frac{r_4}{1+r_1} \right) \left[\frac{1}{\epsilon} + \ln \left(\frac{\mu^2}{n \cdot p (\omega - \bar{n} \cdot p)} \right) - \frac{1}{2} \ln \left(1 - \frac{r_4}{1+r_1} \right) - \ln (1+r_1) \right. \right. \\ &\quad \left. \left. + 1 + \frac{r_1}{1-r_4} \right] + \text{Li}_2 \left(1 - \frac{r_1}{1+r_1-r_4} \right) - \text{Li}_2 \left(\frac{1}{1+r_1} \right) - \frac{r_1 r_4}{1-r_4} \ln \left(\frac{r_1}{1+r_1} \right) \right\} \end{aligned} \quad (108)$$

$$\begin{aligned} I_{6,b} &= \int [dl] \frac{n \cdot l n \cdot (p+l)}{[n \cdot (p+l) \bar{n} \cdot (p-k+l) + l_\perp^2 - m_c^2 + i0][n \cdot l \bar{n}(l-k) + l_\perp^2 + i0][l^2 + i0]} \\ &= \frac{n \cdot p}{2\omega} \left\{ \left(\frac{r_1^2}{(1-r_4)^2} - 1 \right) \ln (1-r_4+r_1) + (1-r_1^2) \ln (1+r_1) - \frac{r_1^2 r_4 (2-r_4)}{(1-r_4)^2} \ln r_1 \right. \\ &\quad \left. - \frac{r_1 r_4}{1-r_4} \right\} , \end{aligned} \quad (109)$$

where $D = 4 - 2\epsilon$, the integration measure is defined as follows

$$[dl] \equiv \frac{(4\pi)^2}{i} \left(\frac{\mu^2 e^{\gamma_E}}{4\pi} \right)^\epsilon \frac{d^D l}{(2\pi)^D} , \quad (110)$$

and we also introduce the conventions

$$r_1 = \frac{m_c^2}{n \cdot p \bar{n} \cdot (k - p)}, \quad r_2 = -\frac{m_c^2}{p^2}, \quad r_3 = -\frac{\bar{n} \cdot k}{\bar{n} \cdot p}, \quad r_4 = \frac{\bar{n} \cdot k}{\bar{n} \cdot (k - p)}. \quad (111)$$

B Spectral representations

We collect the dispersion representations of various convolution integrals entering the NLL resummation improved factorization formula (55), for the sake of constructing the sum rules of $B \rightarrow D$ form factors given by (62). It needs to point out that we have validated each spectral function by verifying the corresponding dispersion integral numerically.

$$\begin{aligned} & \frac{1}{\pi} \text{Im}_{\omega'} \int_0^\infty \frac{d\omega}{\omega' - \omega - \omega_c + i0} \frac{(1 + r_2 + r_3)^2}{r_3(1 + r_3)} \ln \left(\frac{1 + r_2 + r_3}{1 + r_2} \right) \phi_B^+(\omega) \\ &= -\frac{\omega_c}{\omega'} \ln \left| \frac{\omega_c}{\omega' - \omega_c} \right| \phi_B^+(\omega') - \int_{\omega' - \omega_c}^\infty \frac{d\omega}{\omega} \left[\mathcal{P} \frac{\omega_c}{\omega - \omega'} + 1 \right] \theta(\omega' - \omega_c) \phi_B^+(\omega), \end{aligned} \quad (112)$$

$$\begin{aligned} & \frac{1}{\pi} \text{Im}_{\omega'} \int_0^\infty \frac{d\omega}{\omega' - \omega - \omega_c + i0} \frac{r_2^2 r_3}{1 + r_3} \ln \left(\frac{1 + r_2}{r_2} \right) \phi_B^+(\omega) \\ &= \int_0^\infty d\omega \theta(\omega' - \omega_c) \left\{ \frac{\omega \omega_c}{(\omega + \omega_c)^2} \left[\mathcal{P} \frac{1}{\omega' - \omega - \omega_c} - \frac{1}{\omega'} \right] + \frac{\omega_c}{\omega} \left[\mathcal{P} \frac{1}{\omega - \omega'} + \frac{1}{\omega'} \right] \right. \\ & \quad \left. + \frac{\omega_c^2}{\omega + \omega_c} \frac{1}{\omega'^2} \right\} \phi_B^+(\omega) - \ln \left| \frac{\omega_c - \omega'}{\omega_c} \right| \left\{ - \frac{(\omega' - \omega_c)\omega_c}{\omega'^2} \phi_B^+(\omega' - \omega_c) \theta(\omega' - \omega_c) \right. \\ & \quad \left. + \frac{\omega_c}{\omega'} \phi_B^+(\omega') + \delta'(\omega') \int_0^\infty d\omega \frac{\omega_c^2}{\omega + \omega_c} \phi_B^+(\omega) \right\}, \end{aligned} \quad (113)$$

$$\begin{aligned} & \frac{1}{\pi} \text{Im}_{\omega'} \int_0^\infty \frac{d\omega}{\omega' - \omega - \omega_c + i0} \frac{r_2(r_3 - r_2)}{1 + r_3} \ln r_2 \phi_B^+(\omega) \\ &= \int_0^\infty d\omega \theta(\omega') \left[\frac{\omega - \omega_c}{\omega + \omega_c} \mathcal{P} \frac{1}{\omega' - \omega - \omega_c} - \frac{\omega - \omega_c}{\omega} \mathcal{P} \frac{1}{\omega' - \omega} \right] \phi_B^+(\omega) \\ & \quad + \ln \left(\frac{\omega_c}{\omega'} \right) \left[\frac{2\omega_c - \omega'}{\omega'} \phi_B^+(\omega' - \omega_c) \theta(\omega' - \omega_c) + \frac{\omega' - \omega_c}{\omega'} \phi_B^+(\omega') \right] \\ & \quad - \int_0^\infty d\omega \frac{\omega_c(\omega - \omega_c)}{\omega(\omega + \omega_c)} \phi_B^+(\omega) \frac{d}{d\omega'} \left[\ln \left(\frac{\omega_c}{\omega'} \right) \theta(\omega') \right], \end{aligned} \quad (114)$$

$$\begin{aligned} & \frac{1}{\pi} \text{Im}_{\omega'} \int_0^\infty \frac{d\omega}{\omega' - \omega - \omega_c + i0} r_2 \phi_B^+(\omega) \\ &= \frac{\omega_c}{\omega'} \theta(\omega' - \omega_c) \phi_B^+(\omega' - \omega_c) - \delta(\omega') \int_0^\infty d\omega \frac{\omega_c}{\omega + \omega_c} \phi_B^+(\omega), \end{aligned} \quad (115)$$

$$\frac{1}{\pi} \text{Im}_{\omega'} \int_0^\infty \frac{d\omega}{\omega' - \omega - \omega_c + i0} \frac{1}{\omega'} \frac{(1 + r_2 + r_3)^2}{r_3(1 + r_3)^2} \ln \frac{1 + r_2 + r_3}{1 + r_2} \phi_B^+(\omega)$$

$$= - \int_{\omega' - \omega_c}^{\infty} d\omega \theta(\omega' - \omega_c) \mathcal{P} \frac{1}{\omega' - \omega} \left(1 + \omega_c \frac{d}{d\omega} \right) \frac{\phi_B^+(\omega)}{\omega} \\ + \ln \left| \frac{\omega_c}{\omega' - \omega_c} \right| \left(1 + \omega_c \frac{d}{d\omega'} \right) \frac{\phi_B^+(\omega')}{\omega'} + \frac{\phi_B^+(\omega')}{\omega'} \theta(\omega') - \frac{\phi_B^+(\omega' - \omega_c)}{\omega' - \omega_c} \theta(\omega' - \omega_c), \quad (116)$$

$$\frac{1}{\pi} \text{Im}_{\omega'} \int_0^{\infty} \frac{d\omega}{\omega' - \omega - \omega_c + i0} \frac{1}{\omega'} \frac{r_2 [2(1 + r_3) + r_2(2 + r_3)]}{(1 + r_3)^2} \ln \left(\frac{1 + r_2}{r_2} \right) \phi_B^+(\omega) \\ = \int_0^{\infty} d\omega \theta(\omega' - \omega_c) \left[\frac{\omega}{(\omega + \omega_c)^2} \mathcal{P} \frac{1}{\omega' - \omega - \omega_c} + \frac{1}{\omega} \mathcal{P} \frac{1}{\omega - \omega'} + \frac{\omega_c(2\omega + \omega_c)}{\omega(\omega + \omega_c)^2} \frac{1}{\omega'} \right. \\ \left. - \frac{\omega_c^2}{\omega(\omega + \omega_c)} \frac{1}{\omega'^2} \right] \phi_B^+(\omega) - \int_0^{\infty} d\omega \theta(\omega' - \omega_c) \mathcal{P} \frac{\omega_c}{\omega' - \omega} \frac{d}{d\omega} \frac{\phi_B^+(\omega)}{\omega} \\ - \ln \left| \frac{\omega_c - \omega'}{\omega_c} \right| \left[\frac{\omega_c - \omega'}{\omega'^2} \phi_B^+(\omega' - \omega_c) \theta(\omega' - \omega_c) + \frac{\phi_B^+(\omega')}{\omega'} \right] \\ - \theta(\omega' - \omega_c) \frac{\omega_c}{\omega'} \lim_{\omega \rightarrow 0} \frac{\phi_B^+(\omega)}{\omega} - \omega_c \ln \left| \frac{\omega_c - \omega'}{\omega_c} \right| \frac{d}{d\omega'} \frac{\phi_B^+(\omega')}{\omega'} \\ + \delta'(\omega') \ln \left| \frac{\omega_c - \omega'}{\omega_c} \right| \int_0^{\infty} d\omega \frac{\omega_c^2}{\omega(\omega + \omega_c)} \phi_B^+(\omega), \quad (117)$$

$$\frac{1}{\pi} \text{Im}_{\omega'} \int_0^{\infty} \frac{d\omega}{\omega' - \omega - \omega_c + i0} \frac{1}{\omega'} \frac{r_2}{1 + r_3} \phi_B^+(\omega) \\ = \frac{1}{\omega'} \left[\phi_B^+(\omega' - \omega_c) \theta(\omega' - \omega_c) - \phi_B^+(\omega') \theta(\omega') \right] + \delta(\omega') \int_0^{\infty} d\omega \frac{\omega_c}{\omega(\omega + \omega_c)} \phi_B^+(\omega), \quad (118)$$

$$\frac{1}{\pi} \text{Im}_{\omega'} \int_0^{\infty} \frac{d\omega}{\omega' - \omega - \omega_c + i0} \frac{r_2(1 + r_2 + r_3)}{r_3(1 + r_3)} \ln(1 + r_2 + r_3) \phi_B^+(\omega) \\ = \int_0^{\infty} d\omega \theta(\omega_c + \omega - \omega') \theta(\omega') \frac{\omega_c}{\omega} \mathcal{P} \frac{1}{\omega' - \omega} \phi_B^+(\omega) - \frac{\omega_c}{\omega'} \ln \left(\frac{\omega_c}{\omega'} \right) \phi_B^+(\omega') \theta(\omega'), \quad (119)$$

$$\frac{1}{\pi} \text{Im}_{\omega'} \int_0^{\infty} \frac{d\omega}{\omega' - \omega - \omega_c + i0} \frac{r_2(1 + r_2)}{r_3} \ln(1 + r_2) \phi_B^+(\omega) \\ = \theta(\omega') \theta(\omega_c - \omega') \int_0^{\infty} d\omega \frac{\omega_c}{\omega + \omega_c} \frac{\phi_B^+(\omega)}{\omega' - \omega - \omega_c} - \frac{\omega_c}{\omega'} \ln \left| \frac{\omega' - \omega_c}{\omega'} \right| \phi_B^+(\omega' - \omega_c) \theta(\omega' - \omega_c) \\ + \left[\frac{\theta(\omega') \theta(\omega_c - \omega')}{\omega'} \right]_+ \int_0^{\infty} d\omega \frac{\omega_c^2}{\omega(\omega + \omega_c)} \phi_B^+(\omega), \quad (120)$$

$$\frac{1}{\pi} \text{Im}_{\omega'} \int_0^{\infty} \frac{d\omega}{\omega' - \omega - \omega_c + i0} \frac{r_2^2}{1 + r_3} \ln r_2 \phi_B^+(\omega) \\ = \theta(\omega') \int_0^{\infty} d\omega \left[\frac{\omega_c}{\omega + \omega_c} \mathcal{P} \frac{1}{\omega' - \omega - \omega_c} - \frac{\omega_c}{\omega} \frac{1}{\omega' - \omega} \right] \phi_B^+(\omega)$$

$$\begin{aligned}
& -\frac{\omega_c}{\omega'} \ln \left| \frac{\omega_c}{\omega'} \right| \left[\phi_B^+(\omega' - \omega_c) \theta(\omega' - \omega_c) - \phi_B^+(\omega') \theta(\omega') \right] \\
& + \left\{ \left[\frac{\theta(\omega') \theta(\omega_c - \omega')}{\omega'} \right]_+ + \frac{\theta(\omega' - \omega_c)}{\omega'} \right\} \int_0^\infty d\omega \frac{\omega_c^2}{\omega(\omega + \omega_c)} \phi_B^+(\omega), \tag{121}
\end{aligned}$$

$$\begin{aligned}
& \frac{1}{\pi} \text{Im}_{\omega'} \int_0^\infty \frac{d\omega}{\omega' - \omega - \omega_c + i0} \frac{1 + r_2 + r_3}{(1 + r_3)^2} \frac{r_2^2 - (1 + r_3)^2}{r_3} \ln \frac{1 + r_2 + r_3}{1 + r_2} \phi_B^+(\omega) \\
& = \int_0^\infty d\omega \theta(\omega' - \omega_c) \theta(\omega + \omega_c - \omega') \frac{\phi_B^+(\omega)}{\omega} + \omega_c \left[\frac{\phi_B^+(\omega' - \omega_c)}{\omega' - \omega_c} \theta(\omega' - \omega_c) - \frac{\phi_B^+(\omega')}{\omega'} \theta(\omega') \right] \\
& - \omega_c^2 \ln \left| \frac{\omega_c}{\omega' - \omega_c} \right| \frac{d}{d\omega'} \frac{\phi_B^+(\omega')}{\omega'} + \int_0^\infty d\omega \theta(\omega' - \omega_c) \theta(\omega + \omega_c - \omega') \mathcal{P} \frac{\omega_c^2}{\omega' - \omega} \frac{d}{d\omega} \frac{\phi_B^+(\omega)}{\omega}, \tag{122}
\end{aligned}$$

$$\begin{aligned}
& \frac{1}{\pi} \text{Im}_{\omega'} \int_0^\infty \frac{d\omega}{\omega' - \omega - \omega_c + i0} r_2^2 (r_3 + 2) \frac{1 + r_2 + r_3}{(1 + r_3)^2} \ln \frac{1 + r_2}{r_2} \phi_B^+(\omega) \\
& = \omega_c^2 \left\{ \frac{\theta(\omega' - \omega_c)}{\omega'} \lim_{\omega \rightarrow 0} \frac{\phi_B^+(\omega)}{\omega} + \ln \left| \frac{\omega_c - \omega'}{\omega_c} \right| \frac{d}{d\omega'} \frac{\phi_B^+(\omega')}{\omega'} \right. \\
& + \theta(\omega' - \omega_c) \int_0^\infty d\omega \mathcal{P} \frac{1}{\omega' - \omega} \frac{d}{d\omega} \frac{\phi_B^+(\omega)}{\omega} \\
& \left. + \left[\frac{\theta(\omega' - \omega_c)}{\omega'^2} - \delta'(\omega') \ln \left| \frac{\omega_c - \omega'}{\omega_c} \right| \right] \int_0^\infty d\omega \frac{\phi_B^+(\omega)}{\omega} \right\}, \tag{123}
\end{aligned}$$

$$\begin{aligned}
& \frac{1}{\pi} \text{Im}_{\omega'} \int_0^\infty \frac{d\omega}{\omega' - \omega - \omega_c + i0} \frac{r_2(1 + r_2 + r_3)}{1 + r_3} \phi_B^+(\omega) \\
& = \frac{\omega_c}{\omega'} \phi_B^+(\omega') - \omega_c \delta(\omega') \int_0^\infty d\omega \frac{\phi_B^+(\omega)}{\omega}, \tag{124}
\end{aligned}$$

$$\begin{aligned}
& \frac{1}{\pi} \text{Im}_{\omega'} \int_0^\infty \frac{d\omega}{\omega' - \omega - \omega_c + i0} \ln^2 \left(\frac{\mu^2}{n \cdot p(\omega - \omega')} \right) \phi_B^-(\omega) \\
& = 2 \int_0^\infty d\omega \theta(\omega' - \omega) \ln \left(\frac{\mu^2}{n \cdot p(\omega' - \omega)} \right) \mathcal{P} \frac{1}{\omega' - \omega - \omega_c} \phi_B^-(\omega) \\
& - \left[\ln^2 \left(\frac{\mu^2}{n \cdot p \omega_c} \right) - \pi^2 \right] \phi_B^-(\omega' - \omega_c) \theta(\omega' - \omega_c), \tag{125}
\end{aligned}$$

$$\begin{aligned}
& \frac{1}{\pi} \text{Im}_{\omega'} \int_0^\infty \frac{d\omega}{\omega' - \omega - \omega_c + i0} \ln \left(\frac{(1 + r_2 + r_3)^2}{(1 + r_2)(1 + r_3)} \right) \ln \left(\frac{\mu^2}{n \cdot p(\omega - \omega')} \right) \phi_B^-(\omega) \\
& = - \left[\ln^2 \left| \frac{\omega_c}{\omega' - \omega_c} \right| - \pi^2 \theta(\omega' - \omega_c) \right] \phi_B^-(\omega') \tag{125}
\end{aligned}$$

$$\begin{aligned}
& + \int_0^\infty d\omega \theta(\omega' - \omega) \left[\ln^2 \left| \frac{\omega' - \omega - \omega_c}{\omega' - \omega_c} \right| - \pi^2 \theta(\omega' - \omega_c) \theta(\omega + \omega_c - \omega') \right] \frac{d}{d\omega} \phi_B^-(\omega) \\
& + 2 \int_0^\infty d\omega \theta(\omega' - \omega_c) \theta(\omega + \omega_c - \omega') \ln \left| \frac{\omega' - \omega - \omega_c}{\omega' - \omega_c} \right| \\
& \times \left[\mathcal{P} \frac{1}{\omega' - \omega} + \ln \left| \frac{\mu^2}{n \cdot p (\omega - \omega')} \right| \frac{d}{d\omega} \right] \phi_B^-(\omega) \\
& - \ln \left(\frac{\omega' - \omega_c}{\omega_c} \right) \ln \left(\frac{\mu^2}{n \cdot p \omega_c} \right) \phi_B^-(\omega' - \omega_c) \theta(\omega' - \omega_c) \\
& + \int_0^\infty d\omega \theta(\omega') [\theta(\omega_c - \omega') - \theta(\omega - \omega')] \frac{1}{\omega' - \omega - \omega_c} \ln \left| \frac{\mu^2}{n \cdot p (\omega - \omega')} \right| \phi_B^-(\omega) \\
& + \int_0^\infty d\omega \theta(\omega' - \omega) \mathcal{P} \frac{1}{\omega' - \omega - \omega_c} \ln \left| \frac{\omega' - \omega_c}{\omega' - \omega} \right| \phi_B^-(\omega), \tag{126}
\end{aligned}$$

$$\begin{aligned}
& \frac{1}{\pi} \text{Im}_{\omega'} \int_0^\infty \frac{d\omega}{\omega' - \omega - \omega_c + i0} \frac{r_2}{1 + r_2 + r_3} \ln \left(\frac{\mu^2}{n \cdot p (\omega - \omega')} \right) \phi_B^-(\omega) \\
& = -\omega_c \delta(\omega_c - \omega') \ln \left(\frac{\mu^2}{n \cdot p \omega_c} \right) \phi_B^-(0) - \theta(\omega') \mathcal{P} \frac{\omega_c}{\omega_c - \omega'} \phi_B^-(0) + \phi_B^-(\omega') \theta(\omega') \\
& - \phi_B^-(\omega' - \omega_c) \theta(\omega' - \omega_c) - \omega_c \ln \left(\frac{\mu^2}{n \cdot p \omega_c} \right) \left[\frac{d}{d\omega'} \phi_B^-(\omega' - \omega_c) \right] \theta(\omega' - \omega_c) \\
& + \int_0^\infty d\omega \theta(\omega' - \omega) \mathcal{P} \frac{\omega_c}{\omega' - \omega_c - \omega} \frac{d}{d\omega} \phi_B^-(\omega), \tag{127}
\end{aligned}$$

$$\begin{aligned}
& \frac{1}{\pi} \text{Im}_{\omega'} \int_0^\infty \frac{d\omega}{\omega' - \omega - \omega_c + i0} \ln^2(1 + r_2 + r_3) \phi_B^-(\omega) \\
& = \left[\ln^2 \left(\frac{\omega_c - \omega'}{\omega'} \right) - \frac{\pi^2}{3} \right] \theta(\omega_c - \omega') \theta(\omega') \phi_B^-(0) \\
& + \int_0^\infty d\omega \left[\ln^2 \left(\frac{\omega + \omega_c - \omega'}{\omega'} \right) - \frac{\pi^2}{3} \right] \theta(\omega + \omega_c - \omega') \theta(\omega') \frac{d}{d\omega} \phi_B^-(\omega), \tag{128}
\end{aligned}$$

$$\begin{aligned}
& \frac{1}{\pi} \text{Im}_{\omega'} \int_0^\infty \frac{d\omega}{\omega' - \omega - \omega_c + i0} \ln^2(1 + r_3) \phi_B^-(\omega) \\
& = 2 \int_0^\infty d\omega \ln \left(\frac{\omega - \omega'}{\omega'} \right) \frac{1}{\omega' - \omega - \omega_c} \theta(\omega - \omega') \theta(\omega') \phi_B^-(\omega) \\
& - \ln^2 \left(\frac{\omega_c}{\omega'} \right) \phi_B^-(\omega' - \omega_c) \theta(\omega' - \omega_c), \tag{129}
\end{aligned}$$

$$\frac{1}{\pi} \text{Im}_{\omega'} \int_0^\infty \frac{d\omega}{\omega' - \omega - \omega_c + i0} \ln(1 + r_2 + r_3) \ln(1 + r_3) \phi_B^-(\omega)$$

$$\begin{aligned}
&= \frac{1}{2} \int_0^\infty d\omega \left[\ln^2 \left(\frac{\omega + \omega_c - \omega'}{\omega'} \right) - \pi^2 \right] \theta(\omega - \omega') \theta(\omega') \frac{d}{d\omega} \phi_B^-(\omega) \\
&\quad + \int_0^\infty d\omega \theta(\omega + \omega_c - \omega') \theta(\omega') \ln \left(\frac{\omega + \omega_c - \omega'}{\omega'} \right) \left[\mathcal{P} \frac{1}{\omega - \omega'} + \ln \left| \frac{\omega' - \omega}{\omega'} \right| \frac{d}{d\omega} \right] \phi_B^-(\omega) \\
&\quad + \frac{1}{2} \left[\ln^2 \left(\frac{\omega_c}{\omega'} \right) - \pi^2 \right] \phi_B^-(\omega'), \tag{130}
\end{aligned}$$

$$\begin{aligned}
&\frac{1}{\pi} \text{Im}_{\omega'} \int_0^\infty \frac{d\omega}{\omega' - \omega - \omega_c + i0} \frac{1 + r_2}{r_3} \ln \left(\frac{1 + r_2 + r_3}{1 + r_2} \right) \phi_B^-(\omega) \\
&= \int_0^\infty d\omega \ln \left(\frac{\omega + \omega_c - \omega'}{\omega' - \omega_c} \right) \theta(\omega + \omega_c - \omega') \theta(\omega' - \omega_c) (\omega_c - \omega') \frac{d}{d\omega} \frac{\phi_B^-(\omega)}{\omega}, \tag{131}
\end{aligned}$$

$$\begin{aligned}
&\frac{1}{\pi} \text{Im}_{\omega'} \int_0^\infty \frac{d\omega}{\omega' - \omega - \omega_c + i0} (1 + r_2)^2 \ln(1 + r_2) \phi_B^-(\omega) \\
&= - \left(\frac{\omega' - \omega_c}{\omega'} \right)^2 \ln \left(\frac{\omega' - \omega_c}{\omega'} \right) \phi_B^-(\omega' - \omega_c) \theta(\omega' - \omega_c) \\
&\quad + \int_0^\infty d\omega \left(\frac{\omega}{\omega + \omega_c} \right)^2 \theta(\omega_c - \omega') \theta(\omega') \mathcal{P} \frac{1}{\omega' - \omega - \omega_c} \phi_B^-(\omega) \\
&\quad + \left[\frac{\theta(\omega') \theta(\omega_c - \omega')}{\omega'} \right]_+ \int_0^\infty d\omega \frac{\omega_c (2\omega + \omega_c)}{(\omega + \omega_c)^2} \phi_B^-(\omega) \\
&\quad - \left[\frac{\theta(\omega') \theta(\omega_c - \omega')}{\omega'^2} \right]_{++} \int_0^\infty d\omega \frac{\omega_c^2}{\omega + \omega_c} \phi_B^-(\omega), \tag{132}
\end{aligned}$$

$$\begin{aligned}
&\frac{1}{\pi} \text{Im}_{\omega'} \int_0^\infty \frac{d\omega}{\omega' - \omega - \omega_c + i0} \frac{r_2 [r_2 + 2(1 + r_3)]}{(1 + r_3)^2} \ln(1 + r_2 + r_3) \phi_B^-(\omega) \\
&= -\theta(\omega_c - \omega') \theta(\omega') \ln \left(\frac{\omega_c - \omega'}{\omega'} \right) \phi_B^-(0) - \theta(\omega') \ln \left(\frac{\omega_c}{\omega'} \right) \phi_B^-(\omega') \\
&\quad + \left[\theta(\omega') \theta(\omega_c - \omega') \frac{\omega_c}{\omega'} \right]_+ \phi_B^-(0) - \phi_B^+(\omega') \theta(\omega') + \phi_B^+(\omega' - \omega_c) \theta(\omega' - \omega_c) \\
&\quad - \omega_c \ln \left(\frac{\omega_c}{\omega'} \right) \frac{d}{d\omega'} \phi_B^-(\omega') - \int_0^\infty d\omega \theta(\omega + \omega_c - \omega') \theta(\omega') \left[\ln \left(\frac{\omega + \omega_c - \omega'}{\omega'} \right) \frac{d}{d\omega} \right. \\
&\quad \left. + \mathcal{P} \frac{1}{\omega - \omega'} + \mathcal{P} \frac{\omega_c}{\omega - \omega'} \frac{d}{d\omega} \right] \phi_B^-(\omega), \tag{133}
\end{aligned}$$

$$\begin{aligned}
&\frac{1}{\pi} \text{Im}_{\omega'} \int_0^\infty \frac{d\omega}{\omega' - \omega - \omega_c + i0} \ln(1 + r_2 + r_3) \phi_B^-(\omega) \\
&= \theta(\omega_c - \omega') \theta(\omega') \ln \left(\frac{\omega_c - \omega'}{\omega'} \right) \phi_B^-(0)
\end{aligned}$$

$$+ \int_0^\infty d\omega \theta(\omega + \omega_c - \omega') \theta(\omega') \ln \left(\frac{\omega + \omega_c - \omega'}{\omega'} \right) \frac{d}{d\omega} \phi_B^-(\omega), \quad (134)$$

$$\begin{aligned} & \frac{1}{\pi} \text{Im}_{\omega'} \int_0^\infty \frac{d\omega}{\omega' - \omega - \omega_c + i0} \ln(1 + r_2) \ln(1 + r_3) \phi_B^-(\omega) \\ &= -\ln \left(\frac{\omega' - \omega_c}{\omega'} \right) \ln \left(\frac{\omega_c}{\omega'} \right) \phi_B^-(\omega' - \omega_c) \theta(\omega' - \omega_c) \\ &+ \int_0^\infty d\omega \theta(\omega_c - \omega') \theta(\omega') \frac{1}{\omega' - \omega - \omega_c} \ln \left| \frac{\omega' - \omega}{\omega'} \right| \phi_B^-(\omega) \\ &+ \int_0^\infty d\omega \theta(\omega - \omega') \theta(\omega') \frac{1}{\omega' - \omega - \omega_c} \ln \left| \frac{\omega' - \omega_c}{\omega'} \right| \phi_B^-(\omega), \end{aligned} \quad (135)$$

$$\begin{aligned} & \frac{1}{\pi} \text{Im}_{\omega'} \int_0^\infty \frac{d\omega}{\omega' - \omega - \omega_c + i0} \frac{r_2}{1 + r_2 + r_3} \ln(1 + r_3) \phi_B^-(\omega) \\ &= \phi_B^-(\omega' - \omega_c) \theta(\omega' - \omega_c) - \phi_B^-(\omega') \theta(\omega') - \theta(\omega' - \omega_c) \omega_c \ln \left(\frac{\omega_c}{\omega'} \right) \frac{d}{d\omega'} \phi_B^-(\omega' - \omega_c) \\ &+ \int_0^\infty d\omega \theta(\omega - \omega') \theta(\omega') \frac{\omega_c}{\omega' - \omega - \omega_c} \frac{d}{d\omega} \phi_B^-(\omega), \end{aligned} \quad (136)$$

$$\begin{aligned} & \frac{1}{\pi} \text{Im}_{\omega'} \int_0^\infty \frac{d\omega}{\omega' - \omega - \omega_c + i0} \ln^2(1 + r_2) \phi_B^-(\omega) \\ &= -\ln^2 \left(\frac{\omega' - \omega_c}{\omega'} \right) \phi_B^-(\omega' - \omega_c) \theta(\omega' - \omega_c) \\ &+ 2 \int_0^\infty d\omega \theta(\omega_c - \omega') \theta(\omega') \ln \left(\frac{\omega_c - \omega'}{\omega'} \right) \frac{1}{\omega' - \omega - \omega_c} \phi_B^-(\omega), \end{aligned} \quad (137)$$

$$\begin{aligned} & \frac{1}{\pi} \text{Im}_{\omega'} \int_0^\infty \frac{d\omega}{\omega' - \omega - \omega_c + i0} \frac{r_2 \ln r_2}{1 + r_2 + r_3} \phi_B^-(\omega) \\ &= \omega_c \left[\theta(\omega') \mathcal{P} \frac{1}{\omega' - \omega_c} \phi_B^-(0) - \theta(\omega' - \omega_c) \ln \left(\frac{\omega_c}{\omega'} \right) \frac{d}{d\omega'} \phi_B^-(\omega' - \omega_c) \right. \\ &\quad \left. + \int_0^\infty d\omega \theta(\omega') \mathcal{P} \frac{1}{\omega' - \omega - \omega_c} \frac{d}{d\omega} \phi_B^-(\omega) \right], \end{aligned} \quad (138)$$

$$\begin{aligned} & \frac{1}{\pi} \text{Im}_{\omega'} \int_0^\infty \frac{d\omega}{\omega' - \omega - \omega_c + i0} r_2 \left[\frac{r_2}{(1 + r_3)^2} + \frac{2}{1 + r_3} + r_2 + 2 \right] \ln r_2 \phi_B^-(\omega) \\ &= - \left\{ \left[\frac{\theta(\omega_c - \omega') \theta(\omega')}{\omega'^2} \right]_{++} + \frac{\theta(\omega' - \omega_c)}{\omega'^2} + \delta'(\omega') \ln \left| \frac{\omega_c}{\omega' - \omega_c} \right| \right\} \int_0^\infty d\omega \frac{\omega_c^2}{\omega + \omega_c} \phi_B^-(\omega) \\ &+ \left\{ \left[\frac{\theta(\omega_c - \omega') \theta(\omega')}{\omega'} \right]_+ + \frac{\theta(\omega' - \omega_c)}{\omega'} \right\} \int_0^\infty d\omega \frac{\omega_c (\omega_c + 2\omega)}{(\omega + \omega_c)^2} \phi_B^-(\omega) \end{aligned}$$

$$\begin{aligned}
& + \omega_c \left\{ \left[\frac{\theta(\omega_c - \omega') \theta(\omega')}{\omega'} \right]_+ + \frac{\theta(\omega' - \omega_c)}{\omega'} \right\} \phi_B^-(0) - \ln \left(\frac{\omega_c}{\omega'} \right) \left(1 + \omega_c \frac{d}{d\omega'} \right) \phi_B^-(\omega') \\
& + \int_0^\infty d\omega \theta(\omega') \mathcal{P} \frac{1}{\omega' - \omega} \left(1 + \omega_c \frac{d}{d\omega} \right) \phi_B^-(\omega) \\
& + \ln \left(\frac{\omega_c}{\omega'} \right) \frac{\omega'^2 + 2\omega'\omega_c - \omega_c^2}{\omega'^2} \phi_B^-(\omega' - \omega_c) \theta(\omega' - \omega_c) \\
& - \int_0^\infty d\omega \theta(\omega') \mathcal{P} \frac{1}{\omega' - \omega - \omega_c} \frac{\omega^2 + 4\omega\omega_c + 2\omega_c^2}{(\omega + \omega_c)^2} \phi_B^-(\omega), \tag{139}
\end{aligned}$$

$$\begin{aligned}
& \frac{1}{\pi} \text{Im}_{\omega'} \int_0^\infty \frac{d\omega}{\omega' - \omega - \omega_c + i0} \text{Li}_2 \left(\frac{1 + r_3}{1 + r_2 + r_3} \right) \phi_B^-(\omega) \\
& = \int_0^\infty d\omega \left\{ \left[\frac{\pi^2}{6} + \ln \left(\frac{\omega + \omega_c - \omega'}{\omega' - \omega_c} \right) \ln \left(\frac{\omega + \omega_c - \omega'}{\omega_c} \right) \right] \theta(\omega + \omega_c - \omega') \right. \\
& \quad \left. - \frac{1}{2} \ln^2 \left| \frac{\omega' - \omega - \omega_c}{\omega' - \omega_c} \right| \right\} \theta(\omega' - \omega_c) \frac{d}{d\omega} \phi_B^-(\omega) - \int_0^\infty d\omega \left[\theta(\omega + \omega_c - \omega') \theta(\omega' - \omega_c) \right. \\
& \quad \times \ln \left(\frac{\omega_c}{\omega + \omega_c - \omega'} \right) + \theta(\omega' - \omega - \omega_c) \ln \left(\frac{\omega' - \omega - \omega_c}{\omega' - \omega_c} \right) \left. \right] \mathcal{P} \frac{1}{\omega - \omega'} \phi_B^-(\omega) \\
& + \int_0^\infty d\omega \left[\theta(\omega + \omega_c - \omega') \theta(\omega' - \omega_c) \text{Li}_2 \left(\frac{\omega' - \omega}{\omega' - \omega - \omega_c} \right) \right. \\
& \quad \left. - \theta(\omega' - \omega - \omega_c) \ln \left(\frac{\omega' - \omega}{\omega' - \omega - \omega_c} \right) \ln \left(\frac{\omega' - \omega - \omega_c}{\omega' - \omega_c} \right) \right] \frac{d}{d\omega} \phi_B^-(\omega), \tag{140}
\end{aligned}$$

$$\begin{aligned}
& \frac{1}{\pi} \text{Im}_{\omega'} \int_0^\infty \frac{d\omega}{\omega' - \omega - \omega_c + i0} \text{Li}_2 \left(\frac{1}{1 + r_2} \right) \phi_B^-(\omega) \\
& = \left[\text{Li}_2 \left(\frac{\omega' - \omega_c}{\omega'} \right) - \frac{\pi^2}{3} + \frac{1}{2} \ln^2 \left(\frac{\omega'}{\omega' - \omega_c} \right) \right] \phi_B^-(\omega' - \omega_c) \theta(\omega' - \omega_c) \\
& - \int_0^\infty d\omega \theta(\omega' - \omega_c) \ln \frac{\omega'}{\omega' - \omega_c} \mathcal{P} \frac{1}{\omega' - \omega - \omega_c} \phi_B^-(\omega), \tag{141}
\end{aligned}$$

$$\begin{aligned}
& \frac{1}{\pi} \text{Im}_{\omega'} \int_0^\infty \frac{d\omega}{\omega' - \omega - \omega_c + i0} r_2 \left[\frac{8}{1 + r_2 + r_3} + \frac{1}{1 + r_3} + 1 \right] \phi_B^-(\omega) \\
& = -\delta(\omega') \int_0^\infty d\omega \frac{\omega_c}{\omega + \omega_c} \phi_B^-(\omega) - \phi_B^-(\omega') \theta(\omega') + \frac{\omega' + \omega_c}{\omega'} \phi_B^-(\omega' - \omega_c) \theta(\omega' - \omega_c) \\
& - 8\omega_c \left[\delta(\omega' - \omega_c) \phi_B^-(0) + \frac{d}{d\omega'} \phi_B^-(\omega' - \omega_c) \theta(\omega' - \omega_c) \right], \tag{142}
\end{aligned}$$

where the parameter $\bar{n} \cdot p$ in the definitions of r_2 and r_3 , displayed in (27), should apparently be replaced by ω' in the above convolution integrals. The plus functions are defined as

$$\begin{aligned} \int_{-\infty}^{+\infty} d\omega' [f(\omega')]_+ g(\omega') &= \int_0^\infty d\omega' f(\omega') [g(\omega') - g(0)] , \\ \int_{-\infty}^{+\infty} d\omega' [f(\omega')]_{++} g(\omega') &= \int_0^\infty d\omega' f(\omega') [g(\omega') - g(0) - \omega' g'(0)] . \end{aligned} \quad (143)$$

C The coefficient functions of $\Phi_{-,n}^{\text{eff}}(\omega', \mu)$

We present the coefficient functions $\rho_{-,n}^{(i)}$ ($i = 1, \dots, 7$) entering the “effective” DA $\Phi_{-,n}^{\text{eff}}(\omega', \mu)$ defined in (60).

$$\begin{aligned} \rho_{-,n}^{(1)}(\omega') &= \ln \left(\frac{\mu^2}{n \cdot p \omega_c} \right) \left[2 \ln \left(\frac{\omega' - \omega_c}{\omega_c} \right) - \ln \left(\frac{\mu^2}{n \cdot p \omega_c} \right) \right] - 2 \ln^2 \left(\frac{\omega_c}{\omega'} \right) + \ln^2 \left(\frac{\omega' - \omega_c}{\omega_c} \right) \\ &\quad - \left(1 - \frac{\omega_c}{\omega'} \right)^2 \ln \left(\frac{\omega' - \omega_c}{\omega'} \right) - \frac{\omega'^2 + 2\omega'\omega_c - \omega_c^2}{\omega'^2} \ln \left(\frac{\omega_c}{\omega'} \right) - \frac{\omega_c}{\omega'} + 2 \operatorname{Li}_2 \left(\frac{\omega' - \omega_c}{\omega'} \right) \\ &\quad + \frac{5\pi^2}{6} + 1 , \end{aligned} \quad (144)$$

$$\rho_{-,n}^{(2)}(\omega') = 2\omega_c \left[3 \ln \left(\frac{\mu^2}{n \cdot p \omega_c} \right) + 4 \right] , \quad (145)$$

$$\rho_{-,n}^{(3)}(\omega') = 2 \left[\ln^2 \left| \frac{\omega_c}{\omega' - \omega_c} \right| - \ln^2 \left(\frac{\omega_c}{\omega'} \right) + \pi^2 \theta(\omega_c - \omega') \right] , \quad (146)$$

$$\begin{aligned} \rho_{-,n}^{(4)}(\omega') &= 2\omega_c \delta(\omega_c - \omega') \left[3 \ln \left(\frac{\mu^2}{n \cdot p \omega_c} \right) + 4 \right] - \theta(\omega' - \omega_c) \frac{\omega_c}{\omega'} \\ &\quad + 2 \left[\ln^2 \left(\frac{\omega_c - \omega'}{\omega'} \right) - \ln \left(\frac{\omega_c - \omega'}{\omega'} \right) - \frac{\pi^2}{3} \right] \theta(\omega_c - \omega') \theta(\omega') , \end{aligned} \quad (147)$$

$$\begin{aligned} \rho_{-,n}^{(5)}(\omega, \omega') &= \mathcal{P} \frac{1}{\omega' - \omega - \omega_c} \left\{ 2\theta(\omega' - \omega) \ln \left| \frac{\mu^2}{n \cdot p (\omega' - \omega_c)} \right| + \theta(\omega_c - \omega') \theta(\omega') \left(\frac{\omega}{\omega + \omega_c} \right)^2 \right. \\ &\quad \left. + \theta(\omega') \frac{\omega^2 + 4\omega\omega_c + 2\omega_c^2}{(\omega + \omega_c)^2} - 2\theta(\omega' - \omega_c) \ln \left(\frac{\omega'}{\omega' - \omega_c} \right) \right\} \\ &\quad + \mathcal{P} \frac{1}{\omega - \omega'} \left\{ -4\theta(\omega + \omega_c - \omega') \theta(\omega') \ln \left(\frac{\omega + \omega_c - \omega'}{\omega'} \right) + \theta(\omega') \theta(\omega' - \omega - \omega_c) \right. \\ &\quad \left. + 4\theta(\omega + \omega_c - \omega') \theta(\omega' - \omega_c) \ln \left(\frac{\omega_c}{\omega + \omega_c - \omega'} \right) + 4\theta(\omega' - \omega_c) \ln \left| \frac{\omega' - \omega - \omega_c}{\omega' - \omega_c} \right| \right\} \\ &\quad - 2\theta(\omega') \frac{\theta(\omega_c - \omega') - \theta(\omega - \omega')}{\omega' - \omega - \omega_c} \left(\ln \left| \frac{\mu^2}{n \cdot p (\omega - \omega')} \right| + \ln \left| \frac{\omega' - \omega_c}{\omega'} \right| \right) \end{aligned}$$

$$\begin{aligned}
& + 2 \theta(\omega') \frac{\theta(\omega_c - \omega') + \theta(\omega - \omega')}{\omega' - \omega - \omega_c} \ln \left| \frac{\omega' - \omega}{\omega'} \right| \\
& + \theta(\omega' - \omega_c) \left(\frac{\omega_c}{\omega'^2} - \frac{\omega_c + 2\omega}{\omega + \omega_c} \frac{1}{\omega'} \right) \frac{\omega_c}{\omega + \omega_c} \\
& + \left(\delta(\omega') - \omega_c \ln \left| \frac{\omega_c - \omega'}{\omega_c} \right| \delta'(\omega') \right) \frac{\omega_c}{\omega + \omega_c} \Big\}, \tag{148}
\end{aligned}$$

$$\begin{aligned}
\rho_{-,n}^{(6)}(\omega, \omega') = & -4 \theta(\omega' - \omega_c) \theta(\omega + \omega_c - \omega') \ln \left(\frac{\omega + \omega_c - \omega'}{\omega' - \omega_c} \right) \left[\ln \left| \frac{\mu^2}{n \cdot p(\omega - \omega')} \right| \right. \\
& \left. + \ln \left(\frac{\omega + \omega_c - \omega'}{\omega_c} \right) \right] + 2 \theta(\omega') \theta(\omega + \omega_c - \omega') \theta(\omega' - \omega) \ln^2 \left(\frac{\omega + \omega_c - \omega'}{\omega'} \right) \\
& - 4 \theta(\omega + \omega_c - \omega') \theta(\omega') \ln \left(\frac{\omega + \omega_c - \omega'}{\omega'} \right) \ln \left| \frac{\omega' - \omega}{\omega'} \right| \\
& - 2 \theta(\omega_c + \omega - \omega') \theta(\omega') \ln \left(\frac{\omega + \omega_c - \omega'}{\omega'} \right) - \theta(\omega' - \omega - \omega_c) \theta(\omega') \frac{\omega_c}{\omega' - \omega} \\
& + 2 [\theta(\omega' - \omega_c) - \theta(\omega' - \omega)] \ln^2 \left| \frac{\omega' - \omega - \omega_c}{\omega' - \omega_c} \right| \\
& - 4 \theta(\omega + \omega_c - \omega') \theta(\omega' - \omega_c) \text{Li}_2 \left(\frac{\omega' - \omega}{\omega' - \omega - \omega_c} \right) \\
& + 4 \theta(\omega' - \omega - \omega_c) \ln \left(\frac{\omega' - \omega}{\omega' - \omega - \omega_c} \right) \ln \left(\frac{\omega' - \omega - \omega_c}{\omega' - \omega_c} \right) \\
& + 2 \pi^2 \left[\theta(\omega' - \omega) \theta(\omega' - \omega_c) \theta(\omega + \omega_c - \omega') + \theta(\omega - \omega') \theta(\omega') \right. \\
& \left. - \frac{1}{3} \theta(\omega') \theta(\omega + \omega_c - \omega') \right], \tag{149}
\end{aligned}$$

$$\rho_{-,n}^{(7)}(\omega, \omega') = 2 \theta(\omega + \omega_c - \omega') \theta(\omega' - \omega_c) (\omega_c - \omega') \ln \left(\frac{\omega + \omega_c - \omega'}{\omega' - \omega_c} \right). \tag{150}$$

References

- [1] K. A. Olive *et al.* [Particle Data Group Collaboration], Chin. Phys. C **38** (2014) 090001.
- [2] Y. Amhis *et al.* [Heavy Flavor Averaging Group], arXiv:1612.07233 [hep-ex].
- [3] M. Neubert, Phys. Rept. **245** (1994) 259 [hep-ph/9306320].
- [4] J. A. Bailey *et al.* [MILC Collaboration], Phys. Rev. D **92** (2015) 034506 [arXiv:1503.07237 [hep-lat]].

- [5] H. Na *et al.* [HPQCD Collaboration], Phys. Rev. D **92** (2015) 054510 Erratum: [Phys. Rev. D **93** (2016) 119906] [arXiv:1505.03925 [hep-lat]].
- [6] A. Khodjamirian, T. Mannel and N. Offen, Phys. Lett. B **620** (2005) 52 [hep-ph/0504091].
- [7] A. Khodjamirian, T. Mannel and N. Offen, Phys. Rev. D **75** (2007) 054013 [hep-ph/0611193].
- [8] F. De Fazio, T. Feldmann and T. Hurth, Nucl. Phys. B **733** (2006) 1 Erratum: [Nucl. Phys. B **800** (2008) 405] [hep-ph/0504088].
- [9] F. De Fazio, T. Feldmann and T. Hurth, JHEP **0802** (2008) 031 [arXiv:0711.3999 [hep-ph]].
- [10] S. Faller, A. Khodjamirian, C. Klein and T. Mannel, Eur. Phys. J. C **60** (2009) 603 [arXiv:0809.0222 [hep-ph]].
- [11] H. Boos, T. Feldmann, T. Mannel and B. D. Pecjak, Phys. Rev. D **73** (2006) 036003 [hep-ph/0504005].
- [12] H. Boos, T. Feldmann, T. Mannel and B. D. Pecjak, JHEP **0605** (2006) 056 [hep-ph/0512157].
- [13] P. Gambino, T. Mannel and N. Uraltsev, JHEP **1210** (2012) 169 [arXiv:1206.2296 [hep-ph]].
- [14] M. Beneke, G. Buchalla, M. Neubert and C. T. Sachrajda, Nucl. Phys. B **591** (2000) 313 [hep-ph/0006124].
- [15] Y. M. Wang and Y. L. Shen, Nucl. Phys. B **898** (2015) 563 [arXiv:1506.00667 [hep-ph]].
- [16] I. Z. Rothstein, Phys. Rev. D **70** (2004) 054024 [hep-ph/0301240].
- [17] A. K. Leibovich, Z. Ligeti and M. B. Wise, Phys. Lett. B **564** (2003) 231 [hep-ph/0303099].
- [18] M. Beneke and V. A. Smirnov, Nucl. Phys. B **522** (1998) 321 [hep-ph/9711391].
- [19] Y. M. Wang and Y. L. Shen, JHEP **1602** (2016) 179 [arXiv:1511.09036 [hep-ph]].
- [20] Y. M. Wang, JHEP **1609** (2016) 159 [arXiv:1606.03080 [hep-ph]].
- [21] H. B. Fu, X. G. Wu, H. Y. Han, Y. Ma and T. Zhong, Nucl. Phys. B **884** (2014) 172 [arXiv:1309.5723 [hep-ph]].
- [22] R. H. Li, C. D. Lü and Y. M. Wang, Phys. Rev. D **80** (2009) 014005 [arXiv:0905.3259 [hep-ph]].
- [23] H. n. Li, Phys. Rev. D **52** (1995) 3958 [hep-ph/9412340].
- [24] T. Kurimoto, H. n. Li and A. I. Sanda, Phys. Rev. D **67** (2003) 054028 [hep-ph/0210289].

- [25] Y. Y. Fan, W. F. Wang, S. Cheng and Z. J. Xiao, Chin. Sci. Bull. **59** (2014) 125 [arXiv:1301.6246 [hep-ph]].
- [26] H. n. Li, Y. L. Shen, Y. M. Wang and H. Zou, Phys. Rev. D **83** (2011) 054029 [arXiv:1012.4098 [hep-ph]].
- [27] H. n. Li, Y. L. Shen and Y. M. Wang, Phys. Rev. D **85** (2012) 074004 [arXiv:1201.5066 [hep-ph]].
- [28] H. N. Li, Y. L. Shen and Y. M. Wang, JHEP **1302** (2013) 008 [arXiv:1210.2978 [hep-ph]].
- [29] H. N. Li, Y. L. Shen and Y. M. Wang, JHEP **1401** (2014) 004 [arXiv:1310.3672 [hep-ph]].
- [30] Y. M. Wang, EPJ Web Conf. **112** (2016) 01021 [arXiv:1512.08374 [hep-ph]].
- [31] H. n. Li and Y. M. Wang, JHEP **1506** (2015) 013 [arXiv:1410.7274 [hep-ph]].
- [32] C. Bourrely, I. Caprini and L. Lellouch, Phys. Rev. D **79** (2009) 013008 Erratum: [Phys. Rev. D **82** (2010) 099902] [arXiv:0807.2722 [hep-ph]].
- [33] I. Caprini, L. Lellouch and M. Neubert, Nucl. Phys. B **530** (1998) 153 [hep-ph/9712417].
- [34] A. G. Grozin and M. Neubert, Phys. Rev. D **55** (1997) 272 [hep-ph/9607366].
- [35] M. Beneke and T. Feldmann, Nucl. Phys. B **592** (2001) 3 [hep-ph/0008255].
- [36] G. Bell, T. Feldmann, Y. M. Wang and M. W. Y. Yip, JHEP **1311** (2013) 191 [arXiv:1308.6114 [hep-ph]].
- [37] K. G. Chetyrkin, Phys. Lett. B **404** (1997) 161 [hep-ph/9703278].
- [38] J. A. M. Vermaasen, S. A. Larin and T. van Ritbergen, Phys. Lett. B **405** (1997) 327 [hep-ph/9703284].
- [39] G. Bell and T. Feldmann, JHEP **0804** (2008) 061 [arXiv:0802.2221 [hep-ph]].
- [40] S. Descotes-Genon and N. Offen, JHEP **0905** (2009) 091 [arXiv:0903.0790 [hep-ph]].
- [41] M. Beneke and J. Rohrwild, Eur. Phys. J. C **71** (2011) 1818 [arXiv:1110.3228 [hep-ph]].
- [42] I. I. Balitsky and V. M. Braun, Nucl. Phys. B **311** (1989) 541.
- [43] A. Khodjamirian, T. Mannel, A. A. Pivovarov and Y.-M. Wang, JHEP **1009** (2010) 089 [arXiv:1006.4945 [hep-ph]].
- [44] A. Khodjamirian, T. Mannel and Y. M. Wang, JHEP **1302** (2013) 010 [arXiv:1211.0234 [hep-ph]].
- [45] H. Kawamura, J. Kodaira, C. F. Qiao and K. Tanaka, Phys. Lett. B **523** (2001) 111 Erratum: [Phys. Lett. B **536** (2002) 344] [hep-ph/0109181].

- [46] B. Geyer and O. Witzel, Phys. Rev. D **72** (2005) 034023 [hep-ph/0502239].
- [47] V. M. Braun, A. N. Manashov and N. Offen, Phys. Rev. D **92** (2015) 074044 [arXiv:1507.03445 [hep-ph]].
- [48] S. J. Lee and M. Neubert, Phys. Rev. D **72** (2005) 094028 [hep-ph/0509350].
- [49] T. Feldmann, B. O. Lange and Y. M. Wang, Phys. Rev. D **89** (2014) 114001 [arXiv:1404.1343 [hep-ph]].
- [50] M. Beneke and T. Feldmann, Nucl. Phys. B **685** (2004) 249 [hep-ph/0311335].
- [51] P. Ball, hep-ph/0308249.
- [52] V. M. Braun, D. Y. Ivanov and G. P. Korchemsky, Phys. Rev. D **69** (2004) 034014 [hep-ph/0309330].
- [53] B. O. Lange and M. Neubert, Phys. Rev. Lett. **91** (2003) 102001 [hep-ph/0303082].
- [54] T. Nishikawa and K. Tanaka, Nucl. Phys. B **879** (2014) 110 [arXiv:1109.6786 [hep-ph]].
- [55] S. Aoki *et al.*, arXiv:1607.00299 [hep-lat].
- [56] M. Beneke, A. Maier, J. Piclum and T. Rauh, Nucl. Phys. B **891** (2015) 42 [arXiv:1411.3132 [hep-ph]].
- [57] B. Dehnadi, A. H. Hoang and V. Mateu, JHEP **1508** (2015) 155 [arXiv:1504.07638 [hep-ph]].
- [58] A. Khodjamirian, C. Klein, T. Mannel and N. Offen, Phys. Rev. D **80** (2009) 114005 [arXiv:0907.2842 [hep-ph]].
- [59] Y. M. Wang, arXiv:1609.09813 [hep-ph].
- [60] P. Ball and E. Kou, JHEP **0304** (2003) 029 [hep-ph/0301135].
- [61] C. Bourrely, B. Machet and E. de Rafael, Nucl. Phys. B **189** (1981) 157.
- [62] E. B. Gregory *et al.*, Phys. Rev. Lett. **104** (2010) 022001 [arXiv:0909.4462 [hep-lat]].
- [63] C. G. Boyd, B. Grinstein and R. F. Lebed, Phys. Lett. B **353** (1995) 306 [hep-ph/9504235].
- [64] D. Bigi and P. Gambino, Phys. Rev. D **94** (2016) 094008 [arXiv:1606.08030 [hep-ph]].
- [65] C. DeTar, PoS LeptonPhoton **2015** (2016) 023 [arXiv:1511.06884 [hep-lat]].
- [66] A. Sirlin, Nucl. Phys. B **196** (1982) 83.
- [67] N. Carrasco, V. Lubicz, G. Martinelli, C. T. Sachrajda, N. Tantalo, C. Tarantino and M. Testa, Phys. Rev. D **91** (2015) 074506 [arXiv:1502.00257 [hep-lat]].

- [68] R. Glattauer *et al.* [Belle Collaboration], Phys. Rev. D **93** (2016) 032006 [arXiv:1510.03657 [hep-ex]].
- [69] J. P. Lees *et al.* [BaBar Collaboration], Phys. Rev. D **88** (2013) 072012 [arXiv:1303.0571 [hep-ex]].
- [70] B. Aubert *et al.* [BaBar Collaboration], Phys. Rev. Lett. **104** (2010) 011802 [arXiv:0904.4063 [hep-ex]].
- [71] A. Celis, M. Jung, X. Q. Li and A. Pich, arXiv:1612.07757 [hep-ph].
- [72] J. F. Kamenik and F. Mescia, Phys. Rev. D **78** (2008) 014003 [arXiv:0802.3790 [hep-ph]].
- [73] D. Bećirević, N. Košnik and A. Tayduganov, Phys. Lett. B **716** (2012) 208 [arXiv:1206.4977 [hep-ph]].
- [74] X. Q. Li, Y. D. Yang and X. Zhang, JHEP **1608** (2016) 054 [arXiv:1605.09308 [hep-ph]].
- [75] Y. L. Shen, Y. B. Wei and C. D. Lü, arXiv:1607.08727 [hep-ph].
- [76] Z. Ligeti, M. Papucci and D. J. Robinson, arXiv:1610.02045 [hep-ph].